Limitations in mitochondrial programming restrain the differentiation and maturation of human stem cell-derived β cells

Anne C. Lietzke[1,2], Elizabeth Bealer[3]*, Kelly Crumley[3]*, Jessica King[3]*, Ava M. Stendahl[1], Jie Zhu[1], Gemma L. Pearson[1], Elena Levi-D'Ancona[1,4], Belle Henry-Kanarek[1,4], Emma C. Reck[1], Manikanta Arnipalli[1,8], Vaibhav Sidarala[1], Emily M. Walker[1], Subramaniam Pennathur[1,6,7], Jesper G.S. Madsen[5], Lonnie D. Shea[3], and Scott A. Soleimanpour[1,6,8#]

[1]Division of Metabolism, Endocrinology and Diabetes and Department of Internal Medicine, University of Michigan Medical School, Ann Arbor, Michigan, USA.

[2]Department of Pharmacology Graduate Program, University of Michigan Medical School, Ann Arbor, Michigan, USA.

[3]Department of Biomedical Engineering, University of Michigan School of Engineering, Ann Arbor, Michigan, USA.

[4]Immunology Graduate Program, University of Michigan Medical School, Ann Arbor, Michigan, USA.

[5]Department of Biochemistry and Molecular Biology, University of Southern Denmark, Odense, Denmark

[6]Department of Molecular and Integrative Physiology, University of Michigan, Ann Arbor, Michigan, USA

[7]Division of Nephrology and Department of Internal Medicine, University of Michigan Medical School, Ann Arbor, Michigan, USA

[8]VA Ann Arbor Healthcare System, Ann Arbor, Michigan, USA.

*These authors contributed equally to this work.

[#]Corresponding Author. Scott A. Soleimanpour, MD, 1000 Wall Street, Brehm Tower Room 6329, Ann Arbor, MI 48105, USA. Phone: (734) 763-0528 E-mail: ssol@med.umich.edu

ABSTRACT

Pluripotent stem cell (SC)-derived islets offer hope as a renewable source for β cell replacement for type 1 diabetes (T1D), yet functional and metabolic immaturity may limit their long-term therapeutic potential. Here, we show that limitations in mitochondrial transcriptional programming impede the formation and maturation of SC-derived β (SC-β) cells. Utilizing transcriptomic profiling, assessments of chromatin accessibility, mitochondrial phenotyping, and lipidomics analyses, we observed that SC-β cells exhibit reduced oxidative and mitochondrial fatty acid metabolism compared to primary human islets that are related to limitations in key mitochondrial transcriptional networks. Surprisingly, we found that reductions in glucose-stimulated mitochondrial respiration in SC-islets were not associated with alterations in mitochondrial mass, structure, or genome integrity. In contrast, SC-islets show limited expression of targets of PPARα and PPARγ, which regulate mitochondrial programming, yet whose functions in β cell differentiation are unknown. Importantly, treatment with WY14643, a potent PPARα agonist, induced expression of mitochondrial targets, improved insulin secretion, and increased the formation and maturation of SC-β cells both *in vitro* and following transplantation. Thus, mitochondrial programming promotes the differentiation and maturation of SC-β cells and may be a promising target to improve β cell replacement efforts for T1D.

INTRODUCTION

All forms of diabetes are associated with reduced mass and function of pancreatic islet β-cells, rendering the body unable to produce sufficient insulin to meet metabolic needs[1]. Thus, replacement of insulin-producing β cells remains a primary goal for diabetes therapy. Pluripotent stem cell (SC)-derived islets, which consist of a heterogeneous mixture of β cells, other islet hormone cell types, as well as immature progenitors and polyhormonal cells, are a promising source for β cell replacement, as these cells could be generated at scale to meet the substantial needs for patients with type 1 diabetes (T1D)[2,3]. Directed differentiation of stem cells towards the β cell lineage requires a relatively lengthy (~1 month), complex, multi-stage protocol, including sequential use of small molecules and growth factors, cellular enrichment approaches, and modulation of spatial environments, which support the progression of SCs to progenitor cell types and eventually towards islets[4–8]. Despite the many advances in SC-islet differentiation, these protocols produce insulin^{+} β-like cells that are not fully functional *in vitro* and have limited glucose-stimulated insulin secretion (GSIS) compared to β cells within primary human islets.

Optimal mitochondrial function is essential to maintain GSIS, yet mitochondrial respiration is impaired in SC-islets and is of unclear etiology[5,6,9,10]. Limitations in mitochondrial metabolism of SC-islets also persist following transplantation *in vivo*[6,10,1112]. Further, several key aspects of mitochondrial metabolism in SC-islets, such as mitochondrial fatty acid metabolism, remain unexplored. Mitochondria are vital to the function of metabolic tissues, yet recent studies position mitochondria as more than client organelles tasked with energy production and have also been shown to regulate cell fate[13,14]. However, whether mitochondrial programming can promote the SC-derived β (SC-β) cell lineage is unknown.

Here, we show that limitations in mitochondrial transcriptional programming restrain SC-β cell differentiation, maturation, and metabolism. We observe several alterations in SC-islet mitochondria compared to human islets, including reductions in glucose-stimulated mitochondrial respiration, expression of OXPHOS machinery, and mitochondrial lipid

metabolism. Surprisingly, these effects were not related to reductions in mitochondrial mass, genome integrity, DNA replication, or structure. Rather, transcriptomic profiling throughout differentiation to SC-islets revealed dysregulation of several transcriptional pathways that control programming of mitochondrial oxidative and fatty acid metabolism, including those downstream of the nuclear receptors PPARα and PPARγ[15,16], which have not been previously studied in SC-β cell differentiation. Indeed, treatment of SC-islets with WY14643, a potent PPARα agonist with modest PPARγ activity[17–20], promoted expression of mitochondrial targets, improved insulin secretion, and increased the formation and maturation of SC-β cells both *in vitro* and upon transplantation into immunodeficient mice. Together, our studies here reveal the novel potential for targeting mitochondrial programming to enhance the differentiation and maturation of SC-β cells.

RESULTS

SC-islets are transcriptionally and metabolically immature

We generated SC-islets via directed differentiation of the H1 human embryonic stem (hES) cell line towards a β cell fate utilizing a protocol developed by the Millman laboratory[4] (Fig. 1A). To evaluate changes in transcriptional signatures throughout differentiation, as well as markers of islet maturity, we performed RNA-sequencing (RNA-seq) across all differentiation stages with comparison to human islet preparations from non-diabetic donors (Fig. S1A-D). These studies, as well as immunofluorescence studies, demonstrated that SCs, and ultimately SC-islets, behaved largely as expected throughout differentiation, with expression of stage-specific markers and expression of islet-specific hormones in stage 6 (as well as polyhormonal cells; Fig. 1B-C). SC-islets also exhibited reduced expression of islet hormones, with exception of *GHRL*, lower levels of β and α cell maturation markers, and relative hyporesponsiveness of insulin release to glucose- and KCl-stimulation compared to primary human islets (Fig. 1D-E).

To complement our findings of transcriptional and functional immaturity in SC-islets, we next profiled metabolic endpoints in SC-islets. We first surveyed the glycolytic intermediates pyruvate and lactate by LC-MS, given the high importance of pyruvate utilization in mature β cells[21–24]. We found that stage 5 and stage 6 cells increased pyruvate concentrations in response to glucose stimulation, albeit at lower levels than human islets (Fig. 1F). Moreover, SCs at every stage generated significantly higher quantities of lactate, including in stage 6 cells, as compared to human islets (Fig. 1G). The presence of higher quantities of lactate in SC-islets than human islets could be consistent with previous observations of defects in glycolytic flux, an inability to silence lactate metabolism due to expression of disallowed genes (such as *LDHA*), or due to the inability to switch from primarily glycolytic to oxidative metabolism in immature β cells, all of which have been reported previously[5,6,10,24,25]. We next performed respirometry studies utilizing the recently described Barofuse instrument, which allows for the assessment of respiration in a gas pressure flow-based perifusion style platform[26]. We confirmed that SC-islets did not exhibit glucose-stimulated oxygen consumption as compared to human islets, which has been shown previously[5,6,10] (Fig. 1H). We also observed that SC-islets displayed more sensitivity to the effects of oligomycin and FCCP-exposure than primary human islets, which could possibly represent that SC-islets may not be as uncoupled as primary human islets but could also be related to relative differences in penetration of the compounds (Fig. 1H). Taken together, SC-islets display a signature of transcriptional, functional, and metabolic immaturity.

Mitochondrial DNA content, mass, and architecture in SC-islets are comparable to those of human islets.

Optimal β cell function is highly dependent on mitochondrial quality and health[27–29]. Given our observations of transcriptional, functional, and metabolic immaturity in SC-islets, we profiled mitochondrial mass and structure of SC-islets at different stages of differentiation and human islets to obtain insights into limitations in mitochondrial respiration as recent studies have had

discordant results regarding reductions in mitochondrial mass in SC-islets compared to primary human islets[5,10]. To survey mitochondrial genome integrity, we measured mitochondrial (mt)DNA content, and while we found higher mtDNA content in stage 0 embryonic stem cells, we noted no significant differences between stage 1-6 cells and human islets (Fig. 2A). To next determine if there were deficiencies in mtDNA replication, we evaluated the initiation of first strand replication. In mtDNA replication, first strand synthesis begins with formation of the D-loop. Elongation of the 7S sequence, which is contained in the D-loop, into the nearby region, *Cytb*, signifies committed initiation of first strand replication. We assessed both D-loop formation and first strand replication initiation and found no differences between stage 0-6 cells and human islets (Fig. 2B). We also observed no differences in mitochondrial mass in stage 0-6 cells compared to human islets by use of two complementary approaches; namely, citrate synthase activity and TOM20 protein expression (Fig. 2C-D). To assess mitochondrial ultrastructure, we next performed transmission electron microscopy. While we noted a lower frequency of mature insulin granules, as previously described[5,6,30,31], we did not observe any differences in quantitative measures of mitochondrial architecture in stage 6 SC-β cells compared to primary human β cells (Fig. 2E). Together, these results suggest that limitations in mitochondrial respiration in SC-islets were not a consequence of reduced mitochondrial genome integrity, DNA replication, mass, or structure.

Transcriptomic profiling reveals potential limitations in mitochondrial metabolism in SC-islets

Due to the similarities in mitochondrial genome integrity, DNA replication, mass, and structure between SC-islets and human islets, we next explored potential transcriptional differences that might provide mechanistic insights into limitations in glucose-stimulated mitochondrial respiration in SC-islets. Following a comparison of RNA-seq data between stage 6 SC-islets and human islets, we found that 11,858 genes were significantly differentially expressed,

including 405 genes represented within MitoCarta 3.0[32], a curated set of nuclear and mitochondrial-encoded genes with high confidence of localization to the mitochondria (Fig. 3A). Notably, while we observed dynamic changes in expression of MitoCarta genes throughout differentiation, we noted a subset of highly expressed MitoCarta genes in primary human islets that appeared to remain relatively lowly expressed throughout SC differentiation, including by stage 6 (Fig. 3B). Pathways analysis of differentially expressed MitoCarta genes showed differences in fatty acid metabolism, amino acid metabolism, and oxidative phosphorylation (OXPHOS) (Fig. 3C-D). As there were a greater number of downregulated Mitocarta 3.0 genes in SC-islets compared to human islets, we wanted to understand the possible biological processes associated with these gene targets via the Search Tool for Recurring Instances of Neighboring Genes (STRING) database[33]. Following STRING analysis of significantly downregulated MitoCarta genes from stage 6 SC-islets, gene ontology (GO) enrichment analysis was used to clarify pathways related to connections identified by STRING. Pathways identified were related to mitochondrial translation, the electron transport chain (ETC)-OXPHOS system, and lipid metabolism (Fig. 3E). Collectively, our transcriptomic studies revealed several pathways that could contribute to limitations in mitochondrial metabolism in SC-islets.

Limitations in the OXPHOS machinery and mitochondrial lipid metabolism in SC-islets

We next wished to clarify the specific nature of transcriptional defects affecting mitochondria in SC-islets. An initial question was whether the limitations in SC-islet mitochondria were related to an impairment in the shift of the glycolytic to OXPHOS metabolic program, which was previously observed in human induced pluripotent stem cell (iPSC)-derived islets[11]. While we observed that expression of genes related to glucose transport and glycolysis were enriched in stage 0 pluripotent cells, we did not observe differences in the glycolytic gene expression program between stage 6 SC-islets and human islets (Fig. 4A). We next considered the possibility that mitochondrial impairments in SC-islets could be related to limitations in the β cell OXPHOS

machinery. Indeed, we observed a notable subset of 29 OXPHOS gene targets that were enriched in human islets compared to stage 6 SC-islets (Fig. 4B-C). These upregulated targets in human islets included genes encoding subunits of all 5 ETC complexes, as well as complex assembly factors (Fig. 4B-C). Notably, stage 0 pluripotent cells also had an enrichment of a subset of OXPHOS gene targets compared to stage 1-6 cells; however, these genes appeared to be largely distinct from those upregulated within human islets (Fig. 4B). To confirm that this phenotype was specific to SC-β cells compared to other SC-islet cell types, we re-analyzed data from a recently published single-cell RNA-seq dataset comparing SC-islets and human islets, as it has been observed that the various directed differentiation protocols from independent laboratories produce SC-islets with similar transcriptomic profiles[34,35]. Indeed, we observed that >50% of OXPHOS gene targets were lower in SC-β cells compared to primary human β cells, whereas there was no significant differences in glycolytic gene expression between the groups (Fig. 4D). Reduced expression of OXPHOS genes appeared to be β cell-specific, as we did not find robust differences in SC-β cells compared to primary human β cells (Fig. 4D). Lower expression of ETC and OXPHOS gene targets in SC-β cells was also supported by transcriptomic profiling by others[6]. We next measured expression of subunits of OXPHOS complexes via Western blot and found that their expression was significantly lower in SCs compared to human islets across all differentiation stages (Fig. 4E). Thus, we observed lower expression of components of the OXPHOS machinery in SCs compared to human islets that appear to be distinct from programming of the glycolytic gene network.

While β cells are not classically considered central regulators of physiologic lipid storage and turnover, lipid metabolism and signaling are well-known to be essential for the maintenance of optimal β cell insulin release[36,37]. Importantly, mitochondrial lipid metabolism has not been examined in SC-islets to date. We observed distinct subsets of genes related to fatty acid biosynthesis and β-oxidation that were enriched in human islets but were not increased during differentiation towards stage 6 SC-islets (Fig. 5A-B). Specifically, we found genes encoding key

initial steps in fatty acid biosynthesis and β-oxidation were markedly lower in SC-islets compared to human islets, including *ACACB*[38,39], a key component of acetyl CoA carboxylase, which catalyzes conversion of acetyl CoA to malonyl CoA as an early step in fatty acid biosynthesis, *CPT1A*[38,40], the rate-limiting enzyme of fatty acid oxidation that catalyzes the transfer of the long-chain acyl-CoA ester to carnitine, to allow fatty acids to enter the mitochondrial matrix for oxidation, and *ACAT1*[40,41], which catalyzes the final step of mitochondrial β-oxidation (Fig. 5C).

To assess if differentiating SCs and SC-islets possessed alterations in mitochondrial fatty acid metabolism, we examined acylcarnitine species by LC-MS, as carnitine is a required cofactor for lipid transport into the mitochondria for fatty acid β-oxidation[42]. Notably, we could not detect long-chain acylcarnitines or L-carnitine during differentiation, while these were detectable in human islets (Fig. 5D-E). We next noted low levels of short-chain acylcarnitines throughout SC differentiation, with elevations in C4:0 acylcarnitines by stage 6. However, both short- and long-chain acylcarnitines were significantly reduced throughout differentiation to SC-islets when compared to human islets (Fig. 5E). Furthermore, we observed lower expression of *ALDH9A1*, a gene encoding a carnitine biosynthetic enzyme, as well as in *CPT1A*, the key regulator long-chain acylcarnitine synthesis, in SC-islets compared to human islets, yet other regulators of short-chain acylcarnitine synthesis and other genes in the carnitine biosynthetic pathway were not lower in SC-islets (Fig. 5C and 5F). Of note, L-carnitine is not included within either SC-islet[4] or human islet media formulations, thus these differences were unrelated to L-carnitine supplementation (B. Haight, Prodo Laboratories, personal communication as human islet media formulation is proprietary). These data indicate that in addition to limitations in expression of the ETC-OXPHOS system, SC-islets exhibit robust differences in mitochondrial fatty acid metabolism compared to primary human islets.

To ensure our transcriptomic findings were not limited to differentiation of a single hES line, we performed RNA-seq in stage 0-6 cells generated from the HUES8 hES cell line and

compared these results to primary human islets. We again observed the expected expression of stage-specific differentiation markers and limitations of islet hormones and of β and α cell maturation markers in stage 6 cells, similar to our observations in H1 cells (Fig. S2A-C). Further, we observed lower expression of genes encoding subunits of all 5 ETC complexes, complex assembly factors, and key regulators related to fatty acid β-oxidation in stage 6 SC-islets compared to primary human islets (Fig. S2D-F). In sum, these data indicate that SC-islets have several limitations in mitochondrial programming, including within the ETC-OXPHOS system and mitochondrial fatty acid metabolism.

SC-islets display lower expression of PPARα and PPARγ transcriptional targets

Due to the transcriptional differences in the OXPHOS machinery and mitochondrial lipid metabolism, we hypothesized that limitations in key transcriptional pathways might prevent optimal mitochondrial programming in SC-islets. To identify candidate transcriptional regulators, we employed the bioinformatic algorithm Enrichr[43–45] to analyze differentially expressed Mitocarta 3.0 genes between stage 6 SC-islets and human islets (Fig. 6A-B). This analysis yielded several expected findings, including the estrogen-related receptor (ERR) family, PDX1, and PRDM16, which all have been associated with the regulation of β-cell development, as well as several effects on mitochondria, including mitochondrial biogenesis, mitophagy, or induction of oxidative metabolism[11,46–49]. We were also intrigued by the enrichment of PPARα and PPARγ in SC-islets, nuclear receptors that are both tightly connected with mitochondrial function, including the regulation of fatty acid oxidation, mitochondrial biogenesis, and coordination of mitochondrial programming together with the co-activator PGC1α, a central regulator of mitochondrial metabolism[15,16,50]. Thus, we next assessed the expression of PPARα and PPARγ target genes in stage 6 SC-islets and human islets. We found that expression of canonical PPARα and PPARγ target genes were lower in stage 6 SC-islets compared to human islets (Fig.

6C). Further, PPARα regulates carnitine biosynthesis and transcriptionally regulates expression of *ALDH9A1*[51,52], which is also lower in SC-islets compared to human islets, as noted above (Fig. 5F).

We next wished to determine the mechanisms by which PPAR transcriptional pathways are lower in SC-islets. PPARα classically complexes with RXR, and together with PPAR and RXR ligands and transcriptional co-activators, form a transcriptional complex that can bind PPAR response elements to facilitate target gene expression[53]. Thus, we first assessed expression of the PPAR and RXR transcriptional machinery in stage 6 SC-islets. We found that *PPARA*, *PPARG*, *RXRA*, and *RXRB* expression levels were higher in stage 6 SC-islets compared to human islets (Fig. 6D). Furthermore, the expression of the PPAR-related co-activators *NCOA1*, *EP300*, *EIF4E*, *SRC*, and *CTNND1* were also more highly expressed in stage 6 SC-islets compared to the human islets (Fig. 6D). To determine if these findings also occurred specifically in β cells, we reanalyzed a publicly-available single-cell RNA-seq data set[34] and found that expression of the *PPARA, PPARG, RXRA,* and *RXRG* were significantly higher in SC-β cells compared to primary human β cells (Fig. 6E). Further, while we observed lower expression of (*PPARG1A*/*PGC1α*) in SC-islets, we did not observe differences in *PGC1α* expression between SC-β cells and primary human β cells (Fig. 6D-E). To assess if chromatin accessibility at putative PPAR- and RXR-binding sites was affected in SC-β cells, we next reanalyzed publicly-available single-cell ATAC-seq data from SC-β cells and primary human β cells. We found that PPAR and RXR motifs were highly accessible in SC-β cells compared to primary β cells (Fig. 6F). These results suggest that limitations in the PPARα/γ transcriptional program in SC-β cells was not due to a loss of the PPAR transcriptional machinery or chromatin accessibility.

We next identified a differentiation trajectory of SC-β cells using single-cell RNA-seq and single-cell ATAC-seq data to understand the dynamics of PPARα expression and activity during β cell differentiation. Using single-cell RNA-seq expression data from SC-islet cells, we first

identified a developmental trajectory from immature *INS*$^{+}$ β cells co-expressing the key endocrine progenitor transcription factor *FEV* to more mature β cells with higher *INS* expression and low/absent expression of *FEV* (Fig. S3A-B). This trajectory was extracted and then combined with single-cell RNA-seq data from primary human β cells to compare expression. We then evaluated several β cell transcriptional regulators, observing greater expression in *PDX1* and *PAX6* across the SC-β cell differentiation trajectory (Fig. S4A). Similarly, *PPARγ* expression increased along the SC-β cell differentiation trajectory (Fig. 6G). Despite this, we observed that the PPARγ gene signature score, calculated using the expression of 51 known PPARγ transcriptional targets[54], remained at a lower level than primary human β cells throughout the SC-β cell differentiation trajectory (Fig. 6H). We next used ChromVAR[55], a computational approach to estimate a per-cell bias-corrected measure of the change in chromatin accessibility in sets of peaks containing the same transcription factor motif compared to an average cell, which serves as a proxy for transcription factor activity. Again, an evaluation of known β cell transcriptional activators revealed increases in *NEUROD1* and *PAX6* activity across SC-β cell differentiation trajectory (Fig. S4B). Intriguingly, we observed that the estimated PPARγ activity did not change significantly across the SC-β cell differentiation trajectory but was consistently greater than that of primary β cells (Fig. 6I). Taken together, our analysis of bulk RNA-seq, pseudo-bulk single-cell RNA-seq and single-cell ATAC-seq, and transcriptomic and chromatin accessibility profiling across the SC-β cell differentitation trajectory, all revealed that SC-β cells possess lower expression of target genes within the PPARγ pathway that do not appear to be due to reduced expression of the PPAR transcriptional machinery, accessibility of PPAR-binding motifs, or PPARγ activity.

WY14643 improves the formation and maturation of SC-β cells

While the actions of PPARδ/γ are well known in many cell types, including studies in postnatal β cells[56,57], the importance of PPARδ/γ during β cell differentiation and maturation are unclear. We speculated that the lack of activation of PPARδ/γ-related mitochondrial programming could be related to the lack of PPARδ/γ ligands during SC-islet differentiation. Notably, the primary ligand for RXR is retinoic acid, which is routinely included in SC-islet differentiation protocols[4,58]. Ligand binding to PPARs induces a conformational change that displaces co-repressors and enhances binding to co-activators to promote the expression of target genes[59,60]. PPAR agonists have also been shown to not be required to increase the number of PPARγ-binding sites, suggesting that chromatin accessibility at PPAR motifs in SC-β cells could be maintained and poised for activation in the absence of an agonist[61], consistent with our observations above (Fig. 6F and I). Therefore, we hypothesized that addition of a PPAR agonist may improve SC-β cell maturation.

As a proof of concept, we included WY14643 during stage 6 of the differentiation program (Fig. 7A), as WY14643 is a potent agonist of PPARα with modest PPARγ activity by binding to the ligand binding domain of the receptors[17–20]. Unexpectedly, we found that WY14643 treatment significantly increased the percentage of C-peptide-positive SC-islets without changes to the glucagon-, somatostatin-, or polyhormone-positive cell populations (Figs. 7B-C and S5A). To gain further insight into the mechanisms underlying the expansion of SC-β cells upon PPAR agonism, we performed RNA-seq studies on WY14643-treated SC-islets compared to control-treated SC-islets. Firstly, we observed the expected induction of several PPARα and PPARγ targets in WY14643-treated SC-islets compared to control-treated SC-islets (Fig. 7D). We next observed higher expression of genes previously reported to be highly expressed in mature β cells[62], most notably including *INS*, *UCN3*, *GCK*, and *G6PC2*, in WY14643-treated SC-islets compared to control-treated SC-islets (Fig. 7E). In WY14643-treated SC-islets compared to control-treated SC-islets, we also observed lower expression of

genes reported to be enriched in immature β cells[62], including *EHF* and *HMGB2*, which are associated with early pancreatic development[63,64] (Fig. 7F). In addition, we found greater expression of ETC-OXPHOS-related genes, with minimal changes in expression of genes related to glucose uptake and glycolysis, in WY14643-treated SC-islets compared to control-treated SC-islets (Fig. 7G and S5B). Concordantly, by Western blot analysis we observed that WY14643 treatment resulted in greater expression of the complex I subunit NDUFA9 compared to controls (Fig. 7H). Further, we found that addition of WY14643 significantly improved insulin secretion in SC-islets compared to controls (Fig. 7I), yet the fold induction of insulin secretion by glucose was similar between the groups. Together, these studies suggest that WY14643 improved the formation and maturation of SC-β cells.

We next wanted to determine if the increase in the β cell lineage by WY14643 was durable *in vivo* following transplantation. Thus, we treated SC-islets with WY14643 or vehicle control for 7 days *in vitro* prior to seeding SC-islets on a poly(lactide-*co*-glycolide) (PLG) microporous scaffold prior to transplantation into the epididymal fat pad of immunodeficient NOD-*scid* IL2Rg^{null} (NSG) mice, as the epididymal fat pad rather than the renal subcapsular space is a translationally relevant transplant site[65,66] (Fig. 7J). We then retrieved the scaffolds 10 days posttransplant due to the limited half-life of WY14643, and we did not administer WY14643 *in vivo* to avoid systemic effects of the agonist. Following graft retrieval, we observed SC-islets appeared as expected within the scaffold with recipient cell growth within and surrounding the xenograft (Fig. 7K). Notably, we observed a durable effect of WY14643 on the SC-β cell lineage 10 days post-transplantation, with a significant increase in C-peptide-positive SC-β cells compared with vehicle-treated controls (Fig. 7L-M). Further, we observed that WY14643 did not affect the percentage of somatostatin- or glucagon-positive cells but did lead to a modest reduction in the immature polyhormone-positive cell population post-transplantation (Fig. 7L-M and S5C). Moreover, WY14643 treatment led to a significant increase in insulin content within the explanted scaffold graft compared to vehicle-treated controls (Fig. 7N). We also observed

that WY14643 treatment did not alter the frequency of Ki-67$^+$, C-peptide$^+$ cells, suggesting WY14643 did not enhance SC-β cell replication (Fig. S5D). WY14643 treatment also did not alter mitochondrial morphology in SC-β cells post-transplantation (Fig. S5E-F). Taken together, the addition of a PPAR agonist to stage 6 SC-islets improved the formation and maturation of SC-β cells, which was durable *in vivo* post-transplantation.

DISCUSSION

Here, we reveal a vital importance for mitochondrial programming to promote the formation and maturation of SC-β cells. Our studies elucidate specific mechanisms underlying limitations in SC-β cell mitochondrial metabolism, including reductions in expression and function of the ETC-OXPHOS system and mitochondrial fatty acid metabolism. We observe limitations in glucose-stimulated respiration in SC-islets without alterations in mitochondrial mass, structure, mtDNA content, and mtDNA replication. We identify several candidates that may contribute to limitations in mitochondrial programming during SC-β cell maturation, notably PPARα and PPARγ. We demonstrate that the PPARα and PPARγ transcriptional machinery is intact and chromatin at the sites of PPARα and PPARγ binding motifs is accessible, but expression of PPARα and PPARγ target genes is reduced, suggesting a deficiency of PPAR ligands in the SC-islet differentiation process. To test a proof of concept of the importance of PPAR-mediated programming in SC-β cells, we found that WY14643 treatment improved insulin secretion, increased the frequency of C-peptide-positive SC-β cells *in vitro* and post-transplant within a translationally relevant engraftment site, and enhanced insulin content within SC-islet grafts. Thus, our data reveal a novel and unexpected importance for mitochondrial programming during SC-β cell differentiation and maturation, expanding beyond classical roles for mitochondria solely in β cell bioenergetics.

Our results suggest that the activation of mitochondrial transcriptional programs can expand the SC-β cell lineage and improve maturation. While the synchronistic connections

between mitochondria and cell fate are well appreciated in other tissue types, such as brown adipocytes[67,68], this connection has not been clear during β cell differentiation. Interestingly, PPARδ/γ regulate the differentiation of adipocytes, keratinocytes, bone, and several immune cell types and promote the expression of genes related to lipid metabolism and mitochondrial biogenesis[69–75], yet their function in SC-β cell maturation had not previously been observed. In adult human islets, PPARδ overexpression or treatment with a PPARδ agonist offered protection from lipotoxicity and preserved GSIS[76,77]. Similarly, PPARγ agonists preserved β cell function in humans with T2D and protected human islets from lipotoxicity[56,78–80]. However, a role for mitochondrial programming by PPARδ/γ to promote human β cell differentiation was not examined. Our studies reveal the potential for targeting PPARδ/γ to expand the SC-β cell lineage.

PPARδ/γ are well known regulators of lipid metabolism, and PPARδ is a central regulator of fatty acid oxidation. Beyond their roles in lipid metabolism and mitochondrial biogenesis, emerging studies demonstrate crosstalk between ERRα and PPARα, which could suggest the potential that WY14643 might indirectly support expression of OXPHOS targets through ERRs[15,81]. Our studies define a previously unknown reduction in mitochondrial lipid metabolism in SC-islets with beneficial roles of WY14643 on SC-β cell formation and maturation, as well as OXPHOS gene expression, which appears distinct from the roles of ERRγ to improve SC-β cell GSIS through induction of OXPHOS and suppression of glycolysis[11]. Future studies will be crucial to discriminate both the specific and integrated contribution of each of these highly integrated mitochondrial transcriptional regulators on SC-islet development, including PPARα, PPARγ, ERRγ, and PGC1α. The impact of pharmacologic agonists of ERRγ[82] and specific, partial, or dual agonists of PPARα and PPARγ[83–85], to together improve both SC-β cell differentiation and maturity (through PPARα/γ) and metabolism/GSIS (through ERRγ) will be intriguing to assess for future translational benefit.

Our studies expand upon the metabolic differences observed in SC-islets compared to primary human islets, which have understandably focused to date on glucose metabolism given the pivotal importance of glucose metabolism for β cell insulin secretion. We confirmed that SC-islets do not exhibit glucose-stimulated mitochondrial respiration, similar to the observations of others[6,10]. We noted that SC-islets exhibited both lower oxygen consumption following oligomycin exposure and a higher peak oxygen consumption after the uncoupler FCCP compared to human islets, which had not been observed previously. These effects could be a function of differences of tissue penetration of pharmacologic agents between SC-islets and human islets despite their similar size and appearance. Alternatively, the differences in SC-islet responses to oligomycin and FCCP could be indicative that SC-islets may be more coupled or possibly have reductions in proton leak compared to primary human islets. Primary β cells are known to be remarkably uncoupled, and blockade of adenosine nucleotide translocase (ANT)-mediated basal proton leak impairs GSIS[86–89]. Indeed, SC-islets express significantly lower levels of ANT than primary human islets ($\log_2$FC -0.66, FDR < 0.05). We also observe alterations in mitochondrial acylcarnitine profiles in SC-islets, indicative of limitations in mitochondrial lipid metabolism that may originate due to limitations in mitochondrial programming by PPARα/γ. A recent study demonstrated that elevations in the sphingolipid ceramide limited the maturation of SC-β cells, suggesting that our observations were not a consequence of broad reductions in lipid concentrations[90]. Reduced levels of C3 and C5 acylcarnitines may also reflect alterations in branched chain amino acid metabolism[91], an effect we also observed in SC-islets (Fig. 3D). Notably, fluctuations in amino acid availability at birth may also impact the nutrient sensitivity of mTORC1 signaling pathway to affect β cell maturation[92]. Unsaturated fatty acids can serve as endogenous ligands for PPARα and/or PPARγ, leading us to speculate a possible similar role for these metabolites in β cell maturation, especially given the fatty acid composition of maternal breast milk[93–96]. It will be intriguing to test

if future approaches to modulate β cell uncoupling or nutrient exposure will have a beneficial impact on SC-β cell differentiation and maturation.

Our findings support and expand upon the importance of metabolic limitations that occur in the generation of SC-β cells. Balboa *et al*.[6] observed that SC-islets have lower levels of TCA metabolites and lower ATP/ADP and NAD^+/NADH ratios as compared to human islets. Further, they found that key metabolic genes, including those within the ETC-OXPHOS system and TCA cycle, continue to remain reduced in SC-β cells up to 6 months post-transplantation *in vivo* despite extended *in vitro* maturation, suggesting that SC-β cells continue to possess mitochondrial limitations well after engraftment. Davis *et al*. identified that a metabolic bottleneck in in SC-β cell glycolysis catalyzed by glyceraldehyde 3-phosphate dehydrogenase (GAPDH) and phosphoglycerate kinase (PGK1), which ultimately limits glucose-stimulated metabolic function and insulin release[10]. Yoshihara *et al*. defined the importance for ERRγ in postnatal murine β-cells by activating expression of the oxidative metabolic gene network[11]. Following ERRγ overexpression in human iPSC-derived islets, they observed improvements in GSIS and increases in OXPHOS expression[11]. Our results reinforce the findings in the studies above, noting defects in OXPHOS expression, persistence of aberrant glycolytic metabolism, and limitations in expression of the ERR transcriptional pathway, while clarifying new roles for reductions in mitochondrial fatty acid metabolism as well as OXPHOS mediated at least in part through mitochondrial programming by PPAR□/γ. Our results also demonstrate the novel potential to activate PPAR□/γ as highly druggable targets to improve SC-β cell differentiation and maturation. Taken together, our results corroborate limitations that remain in the formation of SC-β cells and identify new potential routes to overcome these deficits, possibly requiring pharmacologic targeting of several complementary pathways to generate higher quantities of mature and fully functional SC-β cells for enhanced therapeutic use in diabetes.

EXPERIMENTAL MODEL AND SUBJECT DETAILS

Stem cell-derived islets (SC-islets): SC-islets were differentiated from H1 and HUES8 human pluripotent stem cells (hPSCs) using a 6-stage protocol, as reported previously[4,65,66,97]. Briefly, undifferentiated cells were dispersed into single cells, and 5×10^6 cells were seeded in 6-well cell culture treated plates coated with Matrigel (Corning). Cells were cultured for 24 h in mTeSR1 and then cultured in the differentiation media for 6 stages. During each stage, cells received daily media changes with stage-specific basal media supplemented with growth factors and small molecules to induce differentiation. The stages of this protocol are defined as definitive endoderm (stage 1), primitive gut tube (stage 2), pancreatic progenitor (stages 3 and 4), endocrine progenitor (stage 5) and immature stem cell derived β-cell (stage 6). At the end of each stage, cells could be dissociated from the plate, fixed and analyzed using intracellular flow cytometry for stage-specific biomarkers. These include OCT3/4 (pluripotent cells), SOX17 (definitive endoderm and primitive gut tube cells), PDX1 and NKX6.1 (pancreatic progenitor cells), NXK6.1 and Chromogranin A (endocrine progenitor cells), and NKX6.1 and C-peptide (stem cell derived β-cells). For reaggregation from planar culture, cells were dispersed into single cells using TrypLE and seeded onto suspension culture 6-well plates at 8×10^6 cells per well. Y27632 was included in the media for the first 24 hours of culture, then media was changed every other day for the duration of culture. Plates were placed on an orbital shaker set to 100 rpm inside a humidified incubator. After 3–4 days in culture, reaggregated cell clusters were collected and seeded on the scaffold in the same manner as described above.

Microporous scaffold fabrication: Poly(lactide-*co*-glycolide) (PLG) microporous scaffolds were fabricated as previously described[65]. Briefly, PLG microporous scaffolds were fabricated by compression molding PLG microspheres (75:25 mole ratio d,l-lactide to glycolide) and 250 to 425 μm salt crystals in a 1:30 ratio of PLG microspheres to salt. The mixture was humidified in an incubator for 7 minutes. Scaffolds were compression molded with 77.5 mg of polymer–salt mixture into cylinders 5 mm in diameter by 2 mm in height using a 5 mm KBr die (International

Crystal Laboratories, Garfield, NJ) at 1500 psi for 30 seconds. Molded constructs were gas foamed in 800 psi carbon dioxide for 16 hours in a pressure vessel. The vessel was depressurized at a controlled rate for 30 min. On the day of cell seeding, scaffolds were leached in water for 1.5 hours, changing the water once after 1 hour. Scaffolds were disinfected by submersion in 70% ethanol for 30 seconds and rinsed multiple times with phosphate-buffered saline (PBS).

Scaffold seeding of SC-islets: To initiate scaffold culture differentiations from reaggregated clusters, reaggregated clusters were seeded on scaffolds at a density of 125×10^6 cells/cm^3. Prior to seeding, scaffolds were washed in cell media solution then briefly dried on sterile gauze to improve the absorption of the cell solution into the scaffold. Cells were distributed across both faces of the scaffold and then incubated for 2 hours to allow cell solution to be further absorbed into the scaffold before differentiation media was added.

Human islets: All human samples were procured from de-identified donors without diabetes from the Integrated Islet Distribution Program, Alberta IsletCore, or Prodo Laboratories and approved by the University of Michigan Institutional Review Board. Human primary islets were cultured at 37°C with 5% CO_2 in PIM(S) media (Prodo Laboratories, Aliso Viejo, CA, USA) supplemented with 10% FBS, 100 U/mL penicillin/streptomycin, 100 U/mL antibiotic/antimycotic, and 1 mM PIM(G) (Prodo Laboratories, Aliso Viejo, CA, USA). Islets were used from male and female donors, and donor information is provided in Table S1.

Transplantation of reaggregated SC-islets in immunodeficient mice: SC-islets were transplanted as previously described[65]. All mice were maintained in accordance with the University of Michigan's Institutional Animal Care and Use Committee under specific pathogen-free conditions and were assigned randomly to different experimental groups. Up to 5 mice were housed per cage and were maintained on regular chow with *ad libitum* access to food and water on a 12 h light-dark cycle. An intraperitoneal injection of 150 mg/kg streptozotocin (STZ) was given to 8–10-week-old male NOD.Cg-Prkdc^{scid} Il2rgtm1Wjl/SzJ (NSG) mice (Jackson

Laboratories) 7–10 days prior to transplant. In the days leading up to surgery, blood glucose was monitored using a tail vein prick (Accu-chek). Glucose readings above 300 mg/dL on two consecutive days were considered diabetic. Mice with weight loss less than 20% of body weight and sufficient glucose readings were considered eligible for transplantation. On the day of transplantation, the abdomen was shaved and sterilized. A small incision was made in the peritoneal wall and the epididymal fat pads were unwrapped outside the body. As described above, reaggregated cell clusters were collected and seeded on both faces of the scaffold and incubated at least 2 h before transplantation. Reaggregated cell-laden scaffolds were placed on the fat pads, wrapped in fat pad tissue, and placed back into the peritoneal cavity. Each mouse received approximately 5 million cells in clusters on each scaffold, equaling a total of 10 million cells transplanted per mouse. Mice were sutured, surgically stapled, and received carprofen (0.5 mg/mL) the day of and after surgery. Blood glucose and weights were measured daily for 10 days.

METHOD DETAILS

Static *in vitro* insulin secretion measurements: Static insulin secretion assays on human islets and SC-islets were performed following 1 h incubations with 1.67 mM and 16.7 mM glucose, and 30mM KCl in HEPES-supplemented KRB buffer containing 135 mM NaCl, 4.7 mM KCl, 1.2 mM KH_2PO_4, 5 mM $NaHCO_3$, 1.2 mM $MgSO_4.7H_2O$, 1 mM $CaCl_2$, 10 mM HEPES and 0.1% BSA (pH 7.4). Samples were analyzed for insulin release using Human Insulin Chemiluminescence ELISA (ALPCO; Salem, NH, USA) as per the manufacturer's protocol.

Insulin content of explanted scaffolds: Explanted scaffolds were placed in 9.1 mM HCl 95% EtOH solution. For extraction, samples were sonicated 5x for 15 sec, resting on ice in between sonication periods. Samples were rotated at 4°C overnight. Samples were then spun at 2500 RPM for 30 min at 4°C. Supernatants were stored at -80°C until analysis. Samples were analyzed for insulin release using Human Insulin Chemiluminescence ELISA (ALPCO; Salem, NH, USA) as per the manufacturer's protocol.

Mitochondrial respirometry: The oxygen consumption rate was measured in stage 6 SC-islets and primary human islets using the BaroFuse (EnTox Sciences, INC; Mercer Island, WA, USA) as previously described[26]. 200 islets were placed in Krebs-Ringer Bicarbonate HEPES (KRBH) buffer with a 2 mM glucose per condition. Islets were subject to the following conditions: 20 mM glucose, 10 μM oligomycin (Sigma), 1 μM FCCP (Sigma-Aldrich), and 3 mM KCN (Thermo Scientific) for 60 min each.

Metabolomics: Media was removed, and the cells were washed 1X with ice-cold 150 mM ammonium acetate in LC-MS grade water. Cells were harvested with 200 μL of ice-cold methanol and frozen at -80°C until sample preparation. For extraction, 200 μL of cold water was added to the cells and the cells were scraped. The resulting homogenate was sonicated on ice for 10 sec. 400 μL of chloroform was added. Samples were centrifuged at 17,000 x *g* for 10 min and the resulting top layer was collected and taken to dryness under nitrogen. Samples were reconstituted in 30 μL of 2:1 ACN: water, filtered and 5 μL were injected for analysis. The samples were separated as previously described[98]. LC-MS analysis was performed on the Agilent 6546 quadrupole TOF mass spectrometer, which was coupled to Agilent 1290 LC. The gas temperature was set at 225°C, the drying gas flow at 10 L/min, the nebulizer at 40 psi, the sheath gas temperature at 300°C, and the sheath gas flow at 12 L/min. The Fragmentor (Agilent) was set at 125 V, the skimmer at 65 V, and VCap at 3,000 V. For verification of metabolite identity and retention time, authentic standards of all measured metabolites were run separately and spiked into pooled samples. Metabolites were separated on an InfinityLab Poroshell120 HILIC-Z, 2.7 μm, 2.1 × 150 mm column (Agilent Technologies, CA, USA). Mobile phase A was composed of 90% 10 mM ammonium acetate pH 9.0 with ammonia, 10% acetonitrile (ACN) with 2.5 uM InfinityLab Deactivator Additive (Agilent Technologies, CA, USA) and mobile phase B was composed of 15% 10 mM ammonium acetate pH 9.0 with ammonia, 85% acetonitrile with 2.5 uM InfinityLab Deactivator Additive. The flow rate was 0.25 mL/min, and the gradient was as follows: 0-2 min at 95 % B, 2-5 min at 95% B, 5-5.5 min at 86%, 5.5-8.5

min at 86% B, 8.5-9 min at 84% B, 9-14 min at 84% B, 14-17 min at 80% B, 17-23 min at 60% B, 23-26 min at 60% B, 26-27 min at 95% B, and 27-35 min at 95% B. Column compartment temperature was kept at 25 °C. Data was acquired in negative mode.

Lipidomics: Media was removed, and metabolites were extracted with solvent (8:1:1 ratio of methanol/Chloroform/water) containing stable isotope-labeled internal standards. As previously described[99], an Agilent 6410 triple quadrupole MS system equipped with an Agilent 1200 LC System and an ESI source was utilized. Metabolite separation was achieved using gradient elution on a reverse phase XBridge C18 Column (50 mm × 2.1 mm, 2.5 µm, Waters, Milford, MA, USA) with the corresponding guard column (5 mm x 2.1 mm, 1.7 µm) maintained at 40 °C. LC vials were maintained at 4 °C in a thermostatic autosampler, and the injection volume was set at 4 µL. The mobile phase consisted of solvent A, 5 mM Ammonium Acetate, and solvent B, Acetonitrile. The flow rate was 0.25 mL/min. The gradient elution program was as follows: 0–8.50 min, 2% B; 1.5–9 min, linear gradient from 2% to 50% B; 9–14 min, linear gradient from 50% to 95% B; hold at 95% B for 3 min. The flow rate was 300 µL/min. Acylcarnitine species were each detected by their characteristic LC retention time in the MRM mode following ESI and comparing relative areas with those of corresponding standards. Concentrations of carnitine, acetylcarnitine (C2), propionylcarnitine (C3), butyrylcarnitine (C4), isovalerylcarnitine (C5), hexanoylcarnitine (C6), octanoylcarnitine (C8), myristoylcarnitine (C14), palmitoylcarnitine (C16), and oleoylcarnitine (C18) were calculated by ratios of peak areas of known concentrations of stable isotopically-labeled analogs.

mtDNA content and replication assessments: 25 human islets per donor were handpicked and washed twice with 1X PBS. 100,000 cells from differentiation stage 0 through 6 were washed twice with 1X PBS. Human islets and stem cells were pelleted and stored at -80°C until DNA extraction using the Blood/Tissue DNeasy kit (Qiagen; Germantown, MD, USA) as per manufacturer's instructions. Relative mtDNA content was quantified by qPCR using mtDNA specific primers ND1 (5'-ACCCCCTTCGACCTTGCCGA-3' and 5'-

GGGCCTGCGGCGTATTCGAT-3'), and nuclear DNA specific primers for GAPDH (5'-AATCCCATCACCATCTTCCA-3' and 5'-TGGACTCCACGACGTACTCA-3') as previously described[100]. First-strand mtDNA replication levels were measured by qPCR following digestion by Mnl I, which site specifically digest double-stranded DNA[101,102]. Briefly, primers specific to 7□S mtDNA (5′-ATCAACTGCAACTCCAAAGCCACC-3′ and 5′-TGATTTCACGGAGGATGGTGGTCA-3′), whose amplicon contains a Mnl I site, were used to quantify relative single-stranded mtDNA forming the D-loop. Single-stranded DNA generated from the extension of 7S region was measured using primers specific to CYTB (5′-AGTCCCACCCTCACACGATTCTTT-3′ and 5′-AGTAAGCCGAGGGCCTCTTTGATT-3′), which also contains an Mnl I site. Primers specific to COXI (5′-ACCCTAGACCAAACCTACGCCAAA-3′ and 5′-TAGGCCGAGAAAGTGTTGTGGGAA-3′), whose amplicon does not contain an Mnl I site, were used to quantify non-replicating double-stranded mtDNA. The ratio of 7S or CYTB amplicons to the COXI amplicon were then calculated after qPCR of Mnl I-digested DNA to determine the relative amount of single-stranded mtDNA at the D-loop strand or initiation of first strand replication, respectively.

Citrate synthase activity assay: 1,000 human islets per donor were handpicked and washed twice with 1X PBS. One million cells from differentiation stage 0 through 6 were washed twice with 1X PBS. Human islets and stem cells were lysed with radioimmunoprecipitation assay buffer containing protease and phosphatase inhibitors (Calbiochem), and insoluble material was removed by centrifugation. Lysates \were used to determine citrate synthase activity with the MitoCheck Citrate Synthase Activity Assay Kit (Cayman Chemical, Catalog# 701040) per manufacturer's instructions.

Western blotting: 1,000 human islets per donor were handpicked and washed twice with 1X PBS. One million cells from differentiation stage 0 through 6 were washed twice with 1X PBS. Human islets and stem cells were lysed with radioimmunoprecipitation assay buffer containing protease and phosphatase inhibitors (Calbiochem), and insoluble material was removed by

centrifugation. Equal amounts of proteins were resolved on 4%–20% gradient Tris-glycine gels (Bio-Rad) and transferred to nitrocellulose membranes (Bio-Rad). Membranes were then blocked in 5% milk for 1 h and immunoblotting was performed using antibodies to Vinculin (1:1000; Millipore, Catalog# CP74), Tom20 (1:1000; Cell Signaling Technology, Catalog# 42406), Total OXPHOS Human Antibody Cocktail (1:1000; Abcam, ab110411), NDUFA9 (1:1000; Abcam; ab14713), UQCRC2 (1:1000; Abcam; ab14745), and species-specific HRP-conjugated secondary antibodies (Vector Laboratories).

RNA-seq: Sequencing was performed by the Advanced Genomics Core at University of Michigan Medical School. 250 human islets per donor were handpicked and washed twice with 1X PBS. 250,000 cells from differentiation stage 0 through 6 were washed twice with 1X PBS. Total RNA was isolated from human islet and stem cell samples and DNase treated using commercially available kits (Omega Biotek and Ambion, respectively). Libraries were constructed and subsequently subjected to 151 bp paired-end cycles on the NovaSeq-6000 platform (Illumina). FastQC (v0.11.8) was used to ensure the quality of data. Reads were mapped to the reference genome GRCm38 (ENSEMBL), using STAR (v2.6.1b) and assigned count estimates to genes with RSEM (v1.3.1). Alignment options followed ENCODE standards for RNA-seq. FastQC was used in an additional post-alignment step to ensure that only high-quality data were used for expression quantitation and differential expression. Data were pre-filtered to remove genes with 0 counts in all samples. Differential gene expression analysis was performed using DESeq2, using a negative binomial generalized linear model (thresholds: log2(fold change) >0.5 or <-0.5, FDR (P_{adj}) <0.05). Plots were generated using variations of DESeq2 plotting functions and other packages with Genialis (Boston, MA, USA).

Pathway analysis of differentially expressed genes: Differentially expressed genes for each cell-type were identified using DESeq2 packages with Genialis (Boston, MA, USA). The Kyoto Encyclopedia of Genes and Genomes (KEGG), gene ontology (GO), and WikiPathways databases via both Enrichr and STRING databases were used to determine association with

particular biological processes, diseases, and molecular functions. The top pathways with an FDR-adjusted *p*-value < 5% were summarized in the results.

Transcription factor analysis of differentially expressed genes: Differentially expressed genes for each cell-type were identified using DESeq2 packages with Genialis (Boston, MA, USA). ChIP Enrichment Analysis (ChEA) and TF Perturbations Followed by Expression databases via Enrichr were used to determine association with particular biological processes, diseases, and molecular functions. The top pathways with an FDR-adjusted *p*-value < 5% were summarized in the results.

Analysis of publicly-available scRNA-seq and scATAC-seq[34]: Pseudo-bulk analyses were conducted by comparison of log2 (fold change) between SC-β cells compared to primary β cells. For mapping the SC-β cell differentiation trajectory, we downloaded preprocessed multi-omics (paired scRNA-seq and scATAC-seq) data from SC islets and performed quality control on each modality and sample individually and retained only barcodes that passed quality filtering in both modalities. We embedded the cells using 100 highly variable genes based on the transcriptomic modality only with phate[103] and clustered the cells based on the first 2 phate components. Based on marker genes, we identified trajectories from immature to mature endocrine cell types and extracted the β cell lineage and binned cells along the first phate component. For identification of primary human β cells, we downloaded preprocessed multi-omics (paired scRNA-seq and scATAC-seq) data from primary human islets and performed quality control on each modality and sample individually and retained only barcodes that passed quality filtering in both modalities. We embedded the cells using UMAP based on the first 20 Harmony[104] corrected principal components calculated from 2000 highly variable genes based on the transcriptomic modality. We clustered the cells and based on marker genes, retained only primary human β cells, which we concatenated with the cells extracted from the SC-β cell differentiation trajectory. For estimating motif activity, we called peaked based on the ATAC-seq modality with MACS2[105] using the cells extracted from the SC-β cell differentiation trajectory and

counted fragments in peaks for both primary and SC-β cells using Signac[106]. We identified motifs using the JASPAR2024 database[107], which we used as input for chromVAR[55].

Transmission electron microscopy: Human islets and SC-islets were handpicked, fixed in 3% glutaraldehyde and 3% paraformaldehyde in 0.1 M Cacodylate buffer (CB; pH 7.2) at room temperature for 5 min and then stored at 4 °C. Islets were then washed with PBS and centrifuged at 2000 rpm for 2 min. Pre-warmed 2% agarose solution was then carefully added to islet pellets, centrifuged and allowed to cool at 4 °C for 30 min. Samples were then subjected to osmification in 1.5% K4Fe(CN)6 + 2% OsO4 in 0.1 CB for 1 h, dehydrated by serial washes in EtOH (30%, 50%, 70%, 80%, 90%, 95% and 100%) and embedded in Spurr's resin by polymerization at 60 °C for 24 h. Polymerized resins were then sectioned at 90 nm thickness using a Leica EM UC7 ultramicrotome and imaged at 70 kV using a JEOL 1400 TEM equipped with an AMT CMOS imaging system. Mitochondrial structures (Aspect Ratio, Perimeter, Circularity) were analyzed and quantified by ImageJ.

Immunofluorescence of cryosections: SC-islets and scaffolds containing SC-islets were picked/excised and fixed in 4% paraformaldehyde for 4 h at 4 °C. SC-islets were washed with PBS and centrifuged at 2000 rpm for 2 min. SC-islets were incubated in methylene blue at room temperature for 20 min and then washed 2x with PBS. Excised scaffolds were washed 3x with PBS for 10 min. SC-islets and scaffolds were stored in 30% sucrose in PBS for 16 h at 4 °C . SC-islets and scaffolds were embedded in OCT and frozen at -80 °C and cryosectioned. SC-islet sections were rinsed with 75% EtOH for 5 min at RT to remove methylene blue. SC-islet and scaffold sections were washed 3x with PBS, permeabilized with 0.2% Triton X-100 in PBS for 15 min, washed 3x with PBS and blocked at RT for 1 h with 5% donkey serum in PBT. Primary antibodies were added for 16 h at 4 °C. Primary antibodies raised against C-peptide (1:50; DSHB, Catalog#GN-ID4), Glucagon (1:2000; SantaCruz, Catalog# sc-13091), Glucagon (1:500; Cell Signaling, Catalog#2760), Somatostatin 28 (1:500; Abcam, Catalog#ab111912), Human antigen clone 235-1 (Millipore Sigma; Catalog#MAB1281), OXPHOS (1:100; Abcam,

Catalog#ab110411), and Ki-67 (1:250, Thermo, Catalog#PA5-19462) were used. Sections were then washed 3x with PBS and incubated for 2 h at room temperature with species-specific Dylight405, Cy2, Cy3, and Cy5-conjugated secondary antibodies (Jackson Immunoresearch). Nuclear labelling was performed using DAPI (Invitrogen). Images were captured under 20X and 60X oil immersion magnification on an Olympus IX81 microscope. Immunostained islets were captured with Z-stack images and subjected to deconvolution (CellSens; Olympus). Hormone-positive cells were quantified as hormone-positive cell/total DAPI-positive (*in vitro*) or Human Ag-positive (post-transplantation) cells. Ki-67-positive cells were quantified as Ki-67-positive/total C-peptide-positive cells. Quantification of hormone-positive and Ki-67-positive cells was carried out with blinded samples, and samples were reidentified after quantification to reduce bias. Quantitative 3-D assessments of mitochondrial morphology and network were performed on ImageJ using Mitochondria Analyzer plugin[102,108].

Statistics: In all figures, data are presented as mean ± SEM, and error bars denote SEM, unless otherwise noted in the legends. Statistical comparisons were performed using unpaired two-tailed Student's *t*-tests, one-way or two-way ANOVA, followed by Tukey's or Sidak's post-hoc test for multiple comparisons, as appropriate (GraphPad Prism and R). A P value < 0.05 was considered significant. For transcriptomic profiling, a FDR-corrected P value <0.05 were considered significant (see RNA-seq of SC-islets and human islets above). Outlier tests (ROUT method[109]) were routinely performed in GraphPad Prism, and all results were included in analysis unless designated by the ROUT method.

Data Availability

RNA-seq data have been deposited at GEO (GSE270220) and will be publicly available at the date of publication. Any additional information required to reanalyze the data reported in this paper is available from the lead author on request.

Acknowledgements

S.A.S. acknowledges support from the JDRF (CDA-2016-189, COE-2019-861, SRA-2023-1392), the NIH (R01 DK108921, R01 DK135032, R01 DK135268, R01 DK136671, R01 DK127270, U01 DK127747, P30 DK020572), the Department of Veterans Affairs (I01 BX004444), the Brehm family, and the Anthony family. A.C.L. was supported by the NIH (T32-GM832230). J.L.K. was supported by the National Science Foundation Graduate Research Fellowship (DGE-2241144). G.L.P. was supported by the American Diabetes Association (19-PDF-063). E.L-D. was supported by the NIH (T32-AI007413, T32-AG000114). B.H-K. was supported by the NIH (T32-AI007413, T32-GM145304, F31-DK138544). E.M.W. was supported by the NIH (K01 DK133533). J.G.S.M was supported by the Novo Nordisk Foundation (NNF21OC0068929). S.P. was supported by the JDRF (COE-2019-861) and the NIH (P30DK089503). The JDRF Career Development Award to S.A.S. is partly supported by the Danish Diabetes Academy and the Novo Nordisk Foundation. Next generation sequencing was carried out in the Advanced Genomics Core at the University of Michigan. Human pancreatic islets and/or other resources were provided by the NIDDK-funded Integrated Islet Distribution Program (IIDP) (RRID:SCR _014387) at City of Hope, NIH Grant # U24DK098085. Human islets were also provided by the Alberta Diabetes Institute IsletCore at the University of Alberta in Edmonton (http://www.bcell.org/adi-isletcore.html) with the assistance of the Human Organ Procurement and Exchange (HOPE) program, Trillium Gift of Life Network (TGLN), and other Canadian organ procurement organizations. Islet isolation was approved by the Human Research Ethics Board at the University of Alberta (Pro00013094). All donors' families gave informed consent for the use of pancreatic tissue in research. We thank Drs. K. Claiborn, L. Satin, R. Kennedy, D. Lorberbaum, S. Nowinski, and members of the Soleimanpour laboratory for helpful advice.

Author Contributions

A.C.L. conceived, designed, and performed experiments, interpreted results, drafted, and reviewed the manuscript. J.K., K.C., E.B., A.M.S., J.Z., G.L.P, E.L-D., B.H-K., E.C.R., M.A., V.S., and E.M.W. designed and performed experiments and interpreted results. J.G.S.M., S.P., and L.D.S. designed studies, interpreted results, and reviewed the manuscript. S.A.S. conceived and designed the studies, interpreted results, drafted, edited, and reviewed the manuscript.

Conflict of interest statement

S.A.S has received grant funding from Ono Pharmaceutical Co., Ltd. and is a consultant for Novo Nordisk.

REFERENCES

1. Walker, J. T., Saunders, D. C., Brissova, M. & Powers, A. C. The Human Islet: Mini-Organ With Mega-Impact. *Endocr. Rev.* **42**, 605–657 (2021).
2. Ramzy, A. *et al.* Implanted pluripotent stem-cell-derived pancreatic endoderm cells secrete glucose-responsive C-peptide in patients with type 1 diabetes. *Cell Stem Cell* **28**, 2047-2061.e5 (2021).
3. Reichman, T. W. *et al.* 836-P: Glucose-Dependent Insulin Production and Insulin-Independence in Type 1 Diabetes from Stem Cell–Derived, Fully Differentiated Islet Cells—Updated Data from the VX-880 Clinical Trial. *Diabetes* **72**, 836-P (2023).
4. Hogrebe, N. J., Maxwell, K. G., Augsornworawat, P. & Millman, J. R. Generation of insulin-producing pancreatic β cells from multiple human stem cell lines. *Nat. Protoc.* **16**, 4109–4143 (2021).
5. Nair, G. G. *et al.* Recapitulating endocrine cell clustering in culture promotes maturation of human stem-cell-derived β cells. *Nat. Cell Biol.* **21**, 263–274 (2019).
6. Balboa, D. *et al.* Functional, metabolic and transcriptional maturation of human pancreatic islets derived from stem cells. *Nat. Biotechnol.* **40**, 1042–1055 (2022).
7. Liang, S. *et al.* Differentiation of stem cell-derived pancreatic progenitors into insulin-secreting islet clusters in a multiwell-based static 3D culture system. *Cell Rep. Methods* **3**, 100466 (2023).
8. Sui, L. *et al.* Reduced replication fork speed promotes pancreatic endocrine differentiation and controls graft size. *JCI Insight* **6**, e141553, 141553 (2021).
9. Barsby, T. *et al.* Aberrant metabolite trafficking and fuel sensitivity in human pluripotent stem cell-derived islets. *Cell Rep.* **42**, 112970 (2023).
10. Davis, J. C. *et al.* Glucose Response by Stem Cell-Derived β Cells In Vitro Is Inhibited by a Bottleneck in Glycolysis. *Cell Rep.* **31**, 107623 (2020).

11. Yoshihara, E. *et al.* ERRγ Is Required for the Metabolic Maturation of Therapeutically Functional Glucose-Responsive β Cells. *Cell Metab.* **23**, 622–634 (2016).

12. Augsornworawat, P., Maxwell, K. G., Velazco-Cruz, L. & Millman, J. R. Single-Cell Transcriptome Profiling Reveals β Cell Maturation in Stem Cell-Derived Islets after Transplantation. *Cell Rep.* **32**, 108067 (2020).

13. Picard, M. & Shirihai, O. S. Mitochondrial signal transduction. *Cell Metab.* **34**, 1620–1653 (2022).

14. Han, S. *et al.* Mitochondrial integrated stress response controls lung epithelial cell fate. *Nature* **620**, 890–897 (2023).

15. Fan, W. & Evans, R. PPARs and ERRs: molecular mediators of mitochondrial metabolism. *Curr. Opin. Cell Biol.* **33**, 49–54 (2015).

16. Handschin, C. & Spiegelman, B. M. Peroxisome Proliferator-Activated Receptor γ Coactivator 1 Coactivators, Energy Homeostasis, and Metabolism. *Endocr. Rev.* **27**, 728–735 (2006).

17. Berger, J. & Moller, D. E. The mechanisms of action of PPARs. *Annu. Rev. Med.* **53**, 409–435 (2002).

18. Kamata, S. *et al.* PPARα Ligand-Binding Domain Structures with Endogenous Fatty Acids and Fibrates. *iScience* **23**, 101727 (2020).

19. Willson, T. M., Brown, P. J., Sternbach, D. D. & Henke, B. R. The PPARs: from orphan receptors to drug discovery. *J. Med. Chem.* **43**, 527–550 (2000).

20. Lehmann, J. M. *et al.* An antidiabetic thiazolidinedione is a high affinity ligand for peroxisome proliferator-activated receptor gamma (PPAR gamma). *J. Biol. Chem.* **270**, 12953–12956 (1995).

21. Ainscow, E. K., Zhao, C. & Rutter, G. A. Acute overexpression of lactate dehydrogenase-A perturbs beta-cell mitochondrial metabolism and insulin secretion. *Diabetes* **49**, 1149–1155 (2000).

22. Pullen, T. J. *et al.* Identification of genes selectively disallowed in the pancreatic islet. *Islets* **2**, 89–95 (2010).

23. Sasaki, M. *et al.* Reduction of reactive oxygen species ameliorates metabolism-secretion coupling in islets of diabetic GK rats by suppressing lactate overproduction. *Diabetes* **62**, 1996–2003 (2013).

24. Rutter, G. A., Georgiadou, E., Martinez-Sanchez, A. & Pullen, T. J. Metabolic and functional specialisations of the pancreatic beta cell: gene disallowance, mitochondrial metabolism and intercellular connectivity. *Diabetologia* **63**, 1990–1998 (2020).

25. Iworima, D. G. *et al.* Metabolic switching, growth kinetics and cell yields in the scalable manufacture of stem cell-derived insulin-producing cells. *Stem Cell Res. Ther.* **15**, 1 (2024).

26. Kamat, V. *et al.* A versatile pumpless multi-channel fluidics system for maintenance and real-time functional assessment of tissue and cells. *Cell Rep. Methods* **3**, 100642 (2023).

27. Lowell, B. B. & Shulman, G. I. Mitochondrial dysfunction and type 2 diabetes. *Science* **307**, 384–387 (2005).

28. Pinti, M. V. *et al.* Mitochondrial dysfunction in type 2 diabetes mellitus: an organ-based analysis. *Am. J. Physiol. Endocrinol. Metab.* **316**, E268–E285 (2019).

29. Sangwung, P., Petersen, K. F., Shulman, G. I. & Knowles, J. W. Mitochondrial Dysfunction, Insulin Resistance, and Potential Genetic Implications. *Endocrinology* **161**, bqaa017 (2020).

30. Pagliuca, F. W. *et al.* Generation of Functional Human Pancreatic β Cells In Vitro. *Cell* **159**, 428–439 (2014).

31. Russ, H. A. *et al.* Controlled induction of human pancreatic progenitors produces functional beta-like cells *in vitro*. *EMBO J.* **34**, 1759–1772 (2015).

32. Rath, S. *et al.* MitoCarta3.0: an updated mitochondrial proteome now with sub-organelle localization and pathway annotations. *Nucleic Acids Res.* **49**, D1541–D1547 (2021).

33. Szklarczyk, D. *et al.* The STRING database in 2023: protein-protein association networks and functional enrichment analyses for any sequenced genome of interest. *Nucleic Acids Res.* **51**, D638–D646 (2023).

34. Augsornworawat, P. *et al.* Single-nucleus multi-omics of human stem cell-derived islets identifies deficiencies in lineage specification. *Nat. Cell Biol.* **25**, 904–916 (2023).

35. Schmidt, M. D., Ishahak, M., Augsornworawat, P. & Millman, J. R. Comparative and integrative single cell analysis reveals new insights into the transcriptional immaturity of stem cell-derived β cells. *BMC Genomics* **25**, 105 (2024).

36. Prentki, M., Corkey, B. E. & Madiraju, S. R. M. Lipid-associated metabolic signalling networks in pancreatic beta cell function. *Diabetologia* **63**, 10–20 (2020).

37. Imai, Y., Cousins, R. S., Liu, S., Phelps, B. M. & Promes, J. A. Connecting pancreatic islet lipid metabolism with insulin secretion and the development of type 2 diabetes. *Ann. N. Y. Acad. Sci.* **1461**, 53–72 (2020).

38. Schreurs, M., Kuipers, F. & van der Leij, F. R. Regulatory enzymes of mitochondrial beta-oxidation as targets for treatment of the metabolic syndrome. *Obes. Rev. Off. J. Int. Assoc. Study Obes.* **11**, 380–388 (2010).

39. Wang, Y. *et al.* Acetyl-CoA Carboxylases and Diseases. *Front. Oncol.* **12**, 836058 (2022).

40. Houten, S. M., Violante, S., Ventura, F. V. & Wanders, R. J. A. The Biochemistry and Physiology of Mitochondrial Fatty Acid β-Oxidation and Its Genetic Disorders. *Annu. Rev. Physiol.* **78**, 23–44 (2016).

41. Hai, Q. & Smith, J. D. Acyl-Coenzyme A: Cholesterol Acyltransferase (ACAT) in Cholesterol Metabolism: From Its Discovery to Clinical Trials and the Genomics Era. *Metabolites* **11**, 543 (2021).

42. Zammit, V. A., Ramsay, R. R., Bonomini, M. & Arduini, A. Carnitine, mitochondrial function and therapy. *Adv. Drug Deliv. Rev.* **61**, 1353–1362 (2009).

43. Chen, E. Y. *et al.* Enrichr: interactive and collaborative HTML5 gene list enrichment analysis tool. *BMC Bioinformatics* **14**, 128 (2013).

44. Kuleshov, M. V. *et al.* Enrichr: a comprehensive gene set enrichment analysis web server 2016 update. *Nucleic Acids Res.* **44**, W90-97 (2016).

45. Xie, Z. *et al.* Gene Set Knowledge Discovery with Enrichr. *Curr. Protoc.* **1**, e90 (2021).

46. Brissova, M. *et al.* Reduction in pancreatic transcription factor PDX-1 impairs glucose-stimulated insulin secretion. *J. Biol. Chem.* **277**, 11225–11232 (2002).

47. Gauthier, B. R. *et al.* PDX1 deficiency causes mitochondrial dysfunction and defective insulin secretion through TFAM suppression. *Cell Metab.* **10**, 110–118 (2009).

48. Seale, P. *et al.* Transcriptional control of brown fat determination by PRDM16. *Cell Metab.* **6**, 38–54 (2007).

49. Sugiyama, T. *et al.* Reconstituting pancreas development from purified progenitor cells reveals genes essential for islet differentiation. *Proc. Natl. Acad. Sci. U. S. A.* **110**, 12691–12696 (2013).

50. Finck, B. N. & Kelly, D. P. PGC-1 coactivators: inducible regulators of energy metabolism in health and disease. *J. Clin. Invest.* **116**, 615–622 (2006).

51. Makowski, L. *et al.* Metabolic profiling of PPARalpha-/- mice reveals defects in carnitine and amino acid homeostasis that are partially reversed by oral carnitine supplementation. *FASEB J. Off. Publ. Fed. Am. Soc. Exp. Biol.* **23**, 586–604 (2009).

52. Wen, G., Ringseis, R., Rauer, C. & Eder, K. The mouse gene encoding the carnitine biosynthetic enzyme 4-N-trimethylaminobutyraldehyde dehydrogenase is regulated by peroxisome proliferator-activated receptor α. *Biochim. Biophys. Acta* **1819**, 357–365 (2012).

53. Tahri-Joutey, M. *et al.* Mechanisms Mediating the Regulation of Peroxisomal Fatty Acid Beta-Oxidation by PPARα. *Int. J. Mol. Sci.* **22**, 8969 (2021).

54. Fang, L. *et al.* PPARgene: A Database of Experimentally Verified and Computationally Predicted PPAR Target Genes. *PPAR Res.* **2016**, 1–6 (2016).

55. Schep, A. N., Wu, B., Buenrostro, J. D. & Greenleaf, W. J. chromVAR: inferring transcription-factor-associated accessibility from single-cell epigenomic data. *Nat. Methods* **14**, 975–978 (2017).

56. Gupta, D., Kono, T. & Evans-Molina, C. The role of peroxisome proliferator-activated receptor γ in pancreatic β cell function and survival: therapeutic implications for the treatment of type 2 diabetes mellitus. *Diabetes Obes. Metab.* **12**, 1036–1047 (2010).

57. Onodera, T. *et al.* Protective roles of adiponectin and molecular signatures of HNF4α and PPARα as downstream targets of adiponectin in pancreatic β cells. *Mol. Metab.* **78**, 101821 (2023).

58. Lorberbaum, D. S. *et al.* Retinoic acid signaling within pancreatic endocrine progenitors regulates mouse and human β cell specification. *Dev. Camb. Engl.* **147**, dev189977 (2020).

59. Capelli, D. *et al.* Structural basis for PPAR partial or full activation revealed by a novel ligand binding mode. *Sci. Rep.* **6**, 34792 (2016).

60. Siclari, J. J. & Gardner, K. H. Two steps, one ligand: How PPARγ binds small-molecule agonists. *Struct. Lond. Engl. 1993* **29**, 935–936 (2021).

61. Haakonsson, A. K., Stahl Madsen, M., Nielsen, R., Sandelin, A. & Mandrup, S. Acute Genome-Wide Effects of Rosiglitazone on PPARγ Transcriptional Networks in Adipocytes. *Mol. Endocrinol.* **27**, 1536–1549 (2013).

62. Qiu, W.-L. *et al.* Deciphering Pancreatic Islet β Cell and α Cell Maturation Pathways and Characteristic Features at the Single-Cell Level. *Cell Metab.* **27**, 702 (2018).

63. Ma, Z. *et al.* Deciphering early human pancreas development at the single-cell level. *Nat. Commun.* **14**, 5354 (2023).

64. White, P., Lee May, C., Lamounier, R. N., Brestelli, J. E. & Kaestner, K. H. Defining Pancreatic Endocrine Precursors and Their Descendants. *Diabetes* **57**, 654–668 (2008).

65. Bealer, E. *et al.* Extrahepatic transplantation of 3D cultured stem cell-derived islet organoids on microporous scaffolds. *Biomater. Sci.* **11**, 3645–3655 (2023).

66. Li, F. *et al.* Fas Ligand-Modified Scaffolds Protect Stem Cell Derived β-Cells by Modulating Immune Cell Numbers and Polarization. *ACS Appl. Mater. Interfaces* (2022) doi:10.1021/acsami.2c12939.

67. Seale, P. Transcriptional Regulatory Circuits Controlling Brown Fat Development and Activation. *Diabetes* **64**, 2369–2375 (2015).

68. Cheng, C.-F., Ku, H.-C. & Lin, H. PGC-1α as a Pivotal Factor in Lipid and Metabolic Regulation. *Int. J. Mol. Sci.* **19**, 3447 (2018).

69. Shen, Y. *et al.* Shared PPARα/γ Target Genes Regulate Brown Adipocyte Thermogenic Function. *Cell Rep.* **30**, 3079-3091.e5 (2020).

70. Cristancho, A. G. & Lazar, M. A. Forming functional fat: a growing understanding of adipocyte differentiation. *Nat. Rev. Mol. Cell Biol.* **12**, 722–734 (2011).

71. Mao-Qiang, M. *et al.* Peroxisome-proliferator-activated receptor (PPAR)-gamma activation stimulates keratinocyte differentiation. *J. Invest. Dermatol.* **123**, 305–312 (2004).

72. Hanley, K. *et al.* Keratinocyte differentiation is stimulated by activators of the nuclear hormone receptor PPARalpha. *J. Invest. Dermatol.* **110**, 368–375 (1998).

73. Chougule, A. *et al.* Osteocytes contribute via nuclear receptor PPAR-alpha to maintenance of bone and systemic energy metabolism. *Front. Endocrinol.* **14**, 1145467 (2023).

74. Lazarenko, O. P. *et al.* Rosiglitazone induces decreases in bone mass and strength that are reminiscent of aged bone. *Endocrinology* **148**, 2669–2680 (2007).

75. Christofides, A., Konstantinidou, E., Jani, C. & Boussiotis, V. A. The role of peroxisome proliferator-activated receptors (PPAR) in immune responses. *Metabolism.* **114**, 154338 (2021).

76. Lalloyer, F. *et al.* Peroxisome proliferator-activated receptor alpha improves pancreatic adaptation to insulin resistance in obese mice and reduces lipotoxicity in human islets. *Diabetes* **55**, 1605–1613 (2006).

77. Frigerio, F. *et al.* Peroxisome proliferator-activated receptor alpha (PPARalpha) protects against oleate-induced INS-1E beta cell dysfunction by preserving carbohydrate metabolism. *Diabetologia* **53**, 331–340 (2010).

78. Gastaldelli, A. *et al.* Thiazolidinediones improve β-cell function in type 2 diabetic patients. *Am. J. Physiol.-Endocrinol. Metab.* **292**, E871–E883 (2007).

79. Kahn, S. E. *et al.* Glycemic durability of rosiglitazone, metformin, or glyburide monotherapy. *N. Engl. J. Med.* **355**, 2427–2443 (2006).

80. Lupi, R. *et al.* Rosiglitazone prevents the impairment of human islet function induced by fatty acids: evidence for a role of PPARgamma2 in the modulation of insulin secretion. *Am. J. Physiol. Endocrinol. Metab.* **286**, E560-567 (2004).

81. Desmet, S. J. *et al. Crosstalk Interactions between Transcription Factors ERRα and PPARα Assist PPARα-Mediated Gene Expression*. http://biorxiv.org/lookup/doi/10.1101/2024.01.15.575655 (2024) doi:10.1101/2024.01.15.575655.

82. Yu, D. D. & Forman, B. M. Identification of an agonist ligand for estrogen-related receptors ERRbeta/gamma. *Bioorg. Med. Chem. Lett.* **15**, 1311–1313 (2005).

83. Wright, M. B., Bortolini, M., Tadayyon, M. & Bopst, M. Minireview: Challenges and opportunities in development of PPAR agonists. *Mol. Endocrinol. Baltim. Md* **28**, 1756–1768 (2014).

84. Botta, M. *et al.* PPAR Agonists and Metabolic Syndrome: An Established Role? *Int. J. Mol. Sci.* **19**, 1197 (2018).

85. Gross, B., Pawlak, M., Lefebvre, P. & Staels, B. PPARs in obesity-induced T2DM, dyslipidaemia and NAFLD. *Nat. Rev. Endocrinol.* **13**, 36–49 (2017).

86. Divakaruni, A. S. & Brand, M. D. The Regulation and Physiology of Mitochondrial Proton Leak. *Physiology* **26**, 192–205 (2011).

87. Anwar, M., Kasper, A., Steck, A. R. & Schier, J. G. Bongkrekic Acid-a Review of a Lesser-Known Mitochondrial Toxin. *J. Med. Toxicol. Off. J. Am. Coll. Med. Toxicol.* **13**, 173–179 (2017).

88. Ewart, R. B., Yousufzai, S. Y., Bradford, M. W. & Shrago, E. Rat islet mitochondrial adenine nucleotide translocase and the regulation of insulin secretion. *Diabetes* **32**, 793–797 (1983).

89. Kiranadi, B., Bangham, J. A. & Smith, P. A. Inhibition of electrical activity in mouse pancreatic beta-cells by the ATP/ADP translocase inhibitor, bongkrekic acid. *FEBS Lett.* **283**, 93–96 (1991).

90. Hua, H. *et al.* Remodeling ceramide homeostasis promotes functional maturation of human pluripotent stem cell-derived β cells. *Cell Stem Cell* S1934590924001371 (2024) doi:10.1016/j.stem.2024.04.010.

91. Newgard, C. B. Interplay between lipids and branched-chain amino acids in development of insulin resistance. *Cell Metab.* **15**, 606–614 (2012).

92. Helman, A. *et al.* A Nutrient-Sensing Transition at Birth Triggers Glucose-Responsive Insulin Secretion. *Cell Metab.* **31**, 1004-1016.e5 (2020).

93. Innis, S. M. Polyunsaturated fatty acids in human milk: an essential role in infant development. *Adv. Exp. Med. Biol.* **554**, 27–43 (2004).

94. Schupp, M. & Lazar, M. A. Endogenous ligands for nuclear receptors: digging deeper. *J. Biol. Chem.* **285**, 40409–40415 (2010).

95. Grygiel-Górniak, B. Peroxisome proliferator-activated receptors and their ligands: nutritional and clinical implications--a review. *Nutr. J.* **13**, 17 (2014).

96. Ramiro-Cortijo, D. *et al.* Breast Milk Lipids and Fatty Acids in Regulating Neonatal Intestinal Development and Protecting against Intestinal Injury. *Nutrients* **12**, 534 (2020).

97. Hogrebe, N. J., Augsornworawat, P., Maxwell, K. G., Velazco-Cruz, L. & Millman, J. R. Targeting the cytoskeleton to direct pancreatic differentiation of human pluripotent stem cells. *Nat. Biotechnol.* **38**, 460–470 (2020).

98. Baek, J. *et al.* The deacylase sirtuin 5 reduces malonylation in nonmitochondrial metabolic pathways in diabetic kidney disease. *J. Biol. Chem.* **299**, 102960 (2023).

99. Sas, K. M. *et al.* Tissue-specific metabolic reprogramming drives nutrient flux in diabetic complications. *JCI Insight* **1**, e86976 (2016).

100. Belmonte, F. R. *et al.* Digital PCR methods improve detection sensitivity and measurement precision of low abundance mtDNA deletions. *Sci. Rep.* **6**, 25186 (2016).

101. Karamanlidis, G. *et al.* Defective DNA replication impairs mitochondrial biogenesis in human failing hearts. *Circ. Res.* **106**, 1541–1548 (2010).

102. Sidarala, V. *et al.* Mitofusin 1 and 2 regulation of mitochondrial DNA content is a critical determinant of glucose homeostasis. *Nat. Commun.* **13**, 2340 (2022).

103. Moon, K. R. *et al.* Visualizing structure and transitions in high-dimensional biological data. *Nat. Biotechnol.* **37**, 1482–1492 (2019).

104. Korsunsky, I. *et al.* Fast, sensitive and accurate integration of single-cell data with Harmony. *Nat. Methods* **16**, 1289–1296 (2019).

105. Zhang, Y. *et al.* Model-based Analysis of ChIP-Seq (MACS). *Genome Biol.* **9**, R137 (2008).

106. Stuart, T., Srivastava, A., Madad, S., Lareau, C. A. & Satija, R. Single-cell chromatin state analysis with Signac. *Nat. Methods* **18**, 1333–1341 (2021).

107. Rauluseviciute, I. *et al.* JASPAR 2024: 20th anniversary of the open-access database of transcription factor binding profiles. *Nucleic Acids Res.* **52**, D174–D182 (2024).

108. Chaudhry, A., Shi, R. & Luciani, D. S. A pipeline for multidimensional confocal analysis of mitochondrial morphology, function, and dynamics in pancreatic β-cells. *Am. J. Physiol. Endocrinol. Metab.* **318**, E87–E101 (2020).

109. Motulsky, H. J. & Brown, R. E. Detecting outliers when fitting data with nonlinear regression - a new method based on robust nonlinear regression and the false discovery rate. *BMC Bioinformatics* **7**, 123 (2006).

FIGURE LEGENDS

Figure 1. SC-islets are transcriptionally and metabolically immature. (A) A schematic diagram illustrating the cell stages during differentiation of human pluripotent stem cells (hPSCs) into SC-islets. (B) Differential RNA expression heatmap, displayed as integrated mean $\log_2$ fold change (FC), from RNA-seq data of representative stage marker expression at each differentiation stage (*n* = 4-5 differentiations or independent human islet donors/group). (C) Immunofluorescence images at 60X magnification of stage 6 SC-islets for C-peptide (green), Glucagon (red), Somatostatin (red), and DAPI (blue) (*n* = 3/group). Scale bars, 20 μm. (D) Differential RNA expression heatmap of genes encoding islet cell maturation markers and hormones in stage 6 SC-islets (*n* = 5) and non-diabetic human islet donors (*n* = 6). FC is relative to the average across all individual samples. (E) Insulin secretion following static incubations in 1.67 mM glucose (1.67G), 16.7 mM glucose (16.7G), and 30 mM KCl (30 KCl) normalized to insulin content in stage 6 SC-islets and human islets (*n* = 3 differentiations or independent human islet donors/group); $^*P < 0.05$, $^{**}P < 0.01$ by two-way ANOVA followed by Tukey's multiple comparisons test. Differential metabolomics heatmap demonstrating mean content of pyruvate (F) or lactate (G) at 5 mM glucose (5G) and 20 mM glucose (20G) for differentiation stages 1 through 6 (*n* = 3/group) and human islets (*n* = 5 independent islet donors). (H) Oxygen consumption rate (OCR) fractional change in stage 6 SC-islets (*n* = 4 differentiations) and human islets (*n* = 5 independent islet donors) following exposure to 2 mM glucose (2G), 20 mM glucose (20G), 10 μM oligomycin, 1 μM FCCP, and 3 mM KCN. Data are presented as mean from independent differentiations or donors ± SEM; $^*P < 0.05$, $^{**}P < 0.01$ by unpaired *t*-test of fractional OCR value at designated time point for minimal or maximal respiration by oligomycin or FCCP, respectively.

Figure 2. SC-islets display comparable mitochondrial DNA content, mass, and architecture to human islets. (A) Quantification of ratio of mitochondrial DNA to nuclear DNA

by qPCR for stage 0-6 cells and human islets (*n* = 4/group). (B) Quantification of single strand mitochondrial DNA products measured by qPCR for stage 0-6 cells and human islets (*n* = 3-4/group). (C) Quantification of citrate synthase activity normalized to total protein content for stage 0-6 cells and human islets (*n* = 3-4/group). (D) Representative Western blot (WB) of TOM20 protein expression for stage 0-6 cells and two different human islet donors (left). Vinculin serves as a loading control. Quantification (right) of TOM20 expression (normalized to Vinculin expression) via densitometry of the Western blots (*n* = 4-5/group). (E) Representative transmission electron microscopy (TEM) images of stage 6 SC-β cells and primary human β cells (left) and quantification of mitochondria ultrastructure (right) (*n* = 3/group, ~150 β cell mitochondria scored/sample).

Figure 3. Transcriptomic profiling of SC-islets versus human islets reveals potential limitations in mitochondrial metabolism. (A) Volcano plot depicting differential RNA expression in stage 6 SC-islets compared to human islets (*n* = 6 differentiations or independent human islet donors/group). Significantly differentially expressed genes demarcated by -FDR > 0.5 and |FC| > 1.4. MitoCarta 3.0 genes are highlighted in green. (B) Differential RNA expression heatmaps from RNA-seq data demonstrating expression of significantly differentially expressed MitoCarta 3.0 genes in stage 0-6 cells compared to human islets (*n* = 4-6 differentiations or independent human islet donors/group). FC is relative to the average across all individual samples. Selected terms from Enrichr analysis of differentially expressed MitoCarta genes from stage 6 SC-islets vs. human islets analyzed with the following libraries: (C) KEGG 2021 Human and (D) WikiPathway 2023 Human. (E) STRING analysis of MitoCarta genes with reduced expression in stage 6 SC-islets compared to human islets.

Figure 4. Reduced expression of the OXPHOS machinery in SC-islets. (A) Differential RNA expression heatmap, displayed as integrated mean $\log_2$ fold change (FC), from RNA-seq data of

genes related to glucose transport and glycolysis at each differentiation stage and human islets (*n* = 4-5 differentiations or independent human islet donors/group). (B) Differential RNA expression heatmap (presented as integrated mean/group) of genes encoding OXPHOS components at each differentiation stage as well as human islet donors (*n* = 4-6/group). (C) Differential RNA expression heatmaps from RNAseq demonstrating expression of expression of OXPHOS machinery genes in stage 0-6 cells and human islets (*n* = 4-6 differentiations or independent human islet donors/group). FC is relative to the average across all individual samples. (D) Differential RNA expression heatmap, displayed as integrated mean $\log_2$FC, from scRNA-seq of genes related to glycolysis and glucose transport and OXPHOS between SC-β cells to primary β cells as well as OXPHOS genes between SC-□ cells to primary □ cells. Data curated from Augsornworawat *et al*.[34]. (E) Representative Western blot analysis of expression of OXPHOS subunits, including ATP5A (Complex V), UQCRC2 (Complex III), NDUFA9 (Complex I), SDHB (Complex II), and COXII (Complex IV) in stage 0-6 cells and human islets (left). Vinculin serves as a loading control. Quantification (right) of ATP5A, UQCRC2, NDUFA9, SDHB, and COXII protein expression by densitometry (normalized for Vinculin expression) of the Western blots of stage 0-6 cells and human islets (*n* = 4 differentiations or independent human islet donors/group); $^{*}P < 0.05$, $^{**}P < 0.01$, $^{***}P < 0.001$, by one-way ANOVA followed by Dunnett's multiple comparisons test.

Figure 5. Limitations in mitochondrial lipid metabolism in SC-islets. Differential RNA expression heatmaps from RNA-seq data demonstrating expression of fatty acid biosynthesis (A) or fatty acid β-oxidation (B) genes in stage 0-6 cells and human islets (*n* = 4-6 differentiations or independent human islet donors/group). FC is relative to the average across all individual samples. (C) Differential RNA expression heatmaps from RNA-seq data demonstrating expression of expression of lipid metabolism genes in stage 0-6 cells and human islets (*n* = 3-5 differentiations or independent human islet donors/group). FC is relative to the

average across all individual samples. Lipidomics profiling of (D) L-carnitine (E) and short- or long-chain acylcarnitines (normalized to protein content) for stage 1-6 cells (*n* = 3/group) and human islets (*n* = 4-5 independent islet donors); *$P < 0.05$, **$P < 0.01$, ****$P < 0.0001$ by one-way ANOVA followed by Dunnett's multiple comparisons test. (F) Differential RNA expression heatmaps from RNA-seq data demonstrating expression of expression of carnitine biosynthesis and short- and medium-chain acylcarnitine synthesis genes in stage 0-6 cells and human islets (*n* = 3-5 differentiations or independent human islet donors/group). FC is relative to the average across all individual samples.

Figure 6. SC-islets display reduced expression of PPARα and PPARγ transcriptional targets. Enrichr analysis of significantly differentially expressed genes from stage 6 SC-islets compared to human islets analyzed with the following libraries: (A) ChEA 2022 and (B) Transcription factor (TF) perturbations followed by expression. (C) Differential RNA expression heatmap from RNA-seq data demonstrating integrated mean expression of PPARα targets for stage 6 SC-islets and human islets (*n* = 6/group). (D) Differential RNA expression heatmap from RNA-seq data demonstrating integrated mean expression of genes encoding components of the PPAR-RXR transcriptional binding complex, including transcriptional co-activators, in stage 6 SC-islets and human islets (*n* = 6/group). (E) Differential RNA expression heatmap generated from publicly-available scRNA-seq data[34] demonstrating integrated mean expression of genes encoding components of the PPAR-RXR transcriptional binding complex, including transcriptional co-activators, in SC-β cells and primary β cells. (F) Differential chromatin accessibility heatmap generated from publicly-available scATACseq data[34] demonstrating integrated mean motif accessibility of PPAR and RXR binding sites in SC-β cells and primary β cells. (G) Minimum to maximum box and whisker plots of normalized expression of *PPARA* across SC-β cells differentiation trajectory and primary β cells generated from publicly-available scRNA-seq data[34] (*n* = 3-4 differentiations or independent human islet donors/group). (H)

Minimum to maximum box and whisker plots of PPARA module scores across SC-β cells differentiation trajectory and primary β cells generated from publicly-available scRNA-seq data[34] representing PPARA target gene expression (*n* = 3-4 differentiations or independent human islet donors/group). (I) Minimum to maximum box and whisker plots of motif deviation z-scored across SC-β cells differentiation trajectory and primary β cells generated from publicly-available scATAC-seq data[34] representing PPARα activity (*n* = 3-4 differentiations or independent human islet donors/group).

Figure 7. WY14643 improves the formation and maturation of SC-β cells. (A) A schematic diagram illustrating the use of the potent PPAR agonist with PPARγ activity, WY14643, within the differentiation protocol. (B) Immunofluorescence images at 60X magnification of vehicle control and WY14643-treated stage 6 SC-islets for C-peptide (green), glucagon (red), and DAPI (DNA - blue) (*n* = 3/group). Scale bars, 20 μm. (C) Quantification of C-peptide positive cells, dual hormone-positive cells, either C-peptide and glucagon (GCG) dual-positive or C-peptide and somatostatin (SST) dual-positive, as well as GCG-positive cells, and SST-positive cells by immunostaining in vehicle control and WY14643-treated stage 6 SC-islets (*n* = 3 differentiations/group, ~500 cells quantified/differentiation and respective condition); ***$P < 0.001$ by unpaired Student's *t*-test. (D) Differential RNA expression heatmap (presented as integrated mean/group) of PPAR targets for vehicle control and WY14643-treated stage 6 SC-islets (*n* = 4/group). (E) Differential RNA expression heatmap (presented as integrated mean/group) of mature β cells for vehicle control and WY14643-treated stage 6 SC-islets (*n* = 4/group). (F) Differential RNA expression heatmap (presented as integrated mean/group) of immature β cells for vehicle control and WY14643-treated stage 6 SC-islets (*n* = 4/group). (G) Differential RNA expression heatmap (presented as integrated mean/group) of genes encoding OXPHOS components for vehicle control and WY14643-treated stage 6 SC-islets (*n* = 4/group). (H) Representative Western blot analysis of NDUFA9 protein expression for vehicle control and

WY14643-treated stage 6 SC-islets (top). Vinculin serves as a loading control. Quantification (bottom) of NDUFA9 expression (normalized to Vinculin expression) via densitometry of the Western blots (n = 4/group); *P < 0.05 by unpaired Student's t-test. (I) Insulin secretion following static incubations in 1.67 mM glucose (1.67G), 16.7 mM glucose (16.7G) and 30 mM KCl (30KCl) normalized to insulin content in vehicle control and WY14643-treated stage 6 SC-islets (n = 4 differentiations/group); **P < 0.01 by two-way ANOVA. (J) A schematic diagram illustrating the addition of WY14643 to the differentiation protocol, seeding of SC-islets onto poly(lactide-*co*-glycolide) (PLG) microporous scaffolds, and scaffold transplantation into NSG mice. (K) Immunofluorescence images at 20X and 60X magnification of stage 6 SC-islets for C-peptide (green), human nuclear antigen (red), and DAPI (blue) (n = 3/group). Human nuclear antigen was used to distinguish human transplanted cells from murine recipient cells in the inguinal fat pad. Scale bars, 20 μm. (L) Immunofluorescence images at 60X magnification of vehicle control and WY14643-treated stage 6 SC-islets in explanted scaffold from NSG mice 10 days post-transplant for C-peptide (green), glucagon (red), and DAPI (blue) (n = 3-4/group). Scale bars = 20 μm. (M) Quantification of C-peptide-positive cells only, dual hormone-positive cells, both C-peptide- and GCG- or SST-positive cells, GCG-positive cells, and SST-positive cells by immunostaining in vehicle control and WY14643-treated stage 6 SC-islets in explanted scaffold from NSG mice 10 days post-transplant (n = 3-4/group); *P < 0.05 by unpaired Student's t-test. (N) Insulin content normalized to total protein content for vehicle control and WY14643-treated explanted scaffolds from NSG mice 10 days post-transplant (n = 3-4/group); *P < 0.05 by unpaired Student's t-test.

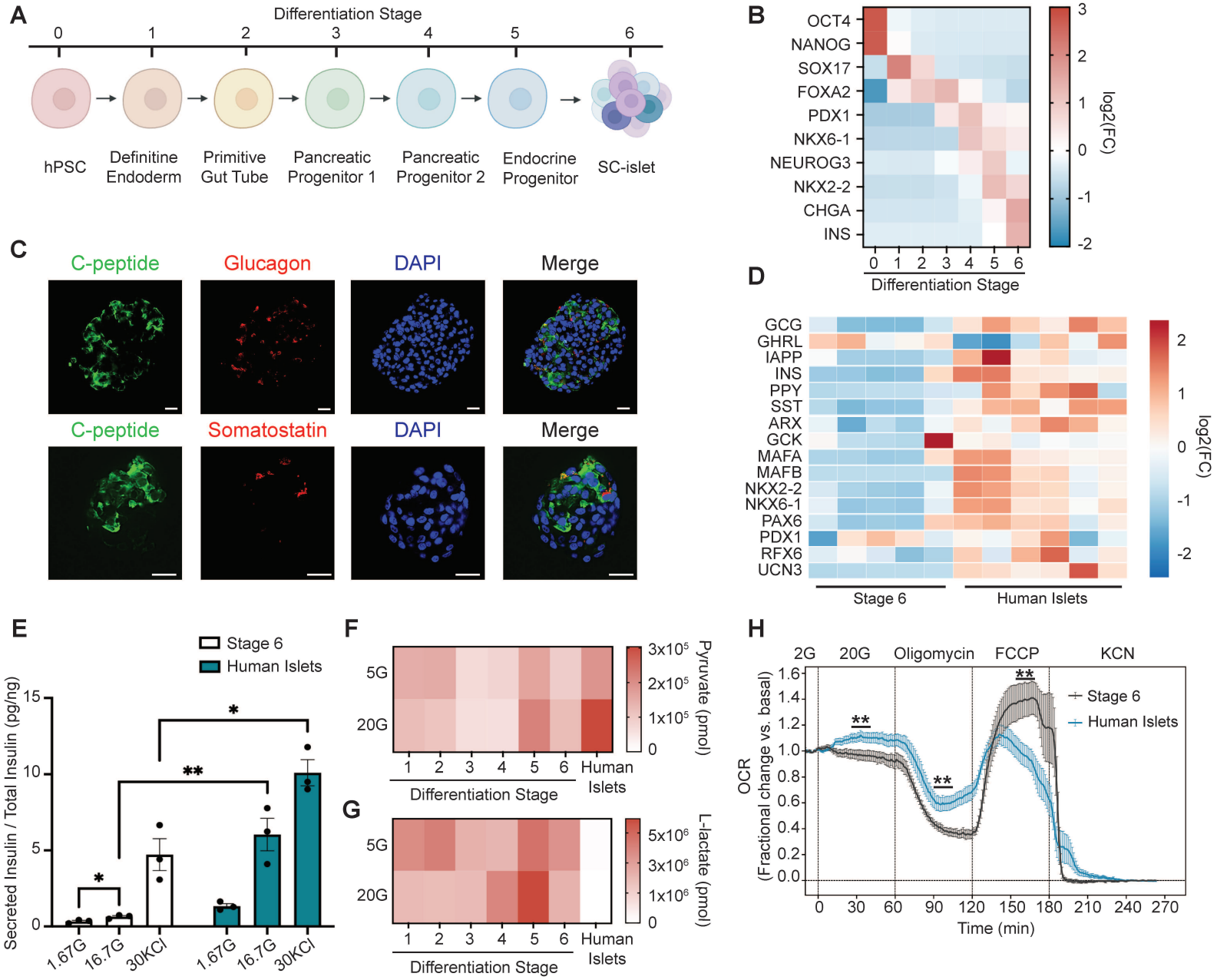
A
Differentiation Stage
0
1
2
3
4
5
6
hPSC
Definitine Endoderm
Primitive Gut Tube
Pancreatic Progenitor 1
Pancreatic Progenitor 2
Endocrine Progenitor
SC-islet
B
OCT4
NANOG
SOX17
FOXA2
PDX1
NKX6-1
NEUROG3
NKX2-2
CHGA
INS
Differentiation Stage
log2(FC)
C
C-peptide
Glucagon
DAPI
Merge
C-peptide
Somatostatin
DAPI
Merge
D
GCG
GHRL
IAPP
INS
PPY
SST
ARX
GCK
MAFA
MAFB
NKX2-2
NKX6-1
PAX6
PDX1
RFX6
UCN3
Stage 6
Human Islets
log2(FC)
E
Stage 6
Human Islets
Secreted Insulin / Total Insulin (pg/ng)
1.67G
16.7G
30KCl
F
5G
20G
Differentiation Stage
Human Islets
Pyruvate (pmol)
G
5G
20G
Differentiation Stage
Human Islets
L-lactate (pmol)
H
2G
20G
Oligomycin
FCCP
KCN
Stage 6
Human Islets
OCR (Fractional change vs. basal)
Time (min)

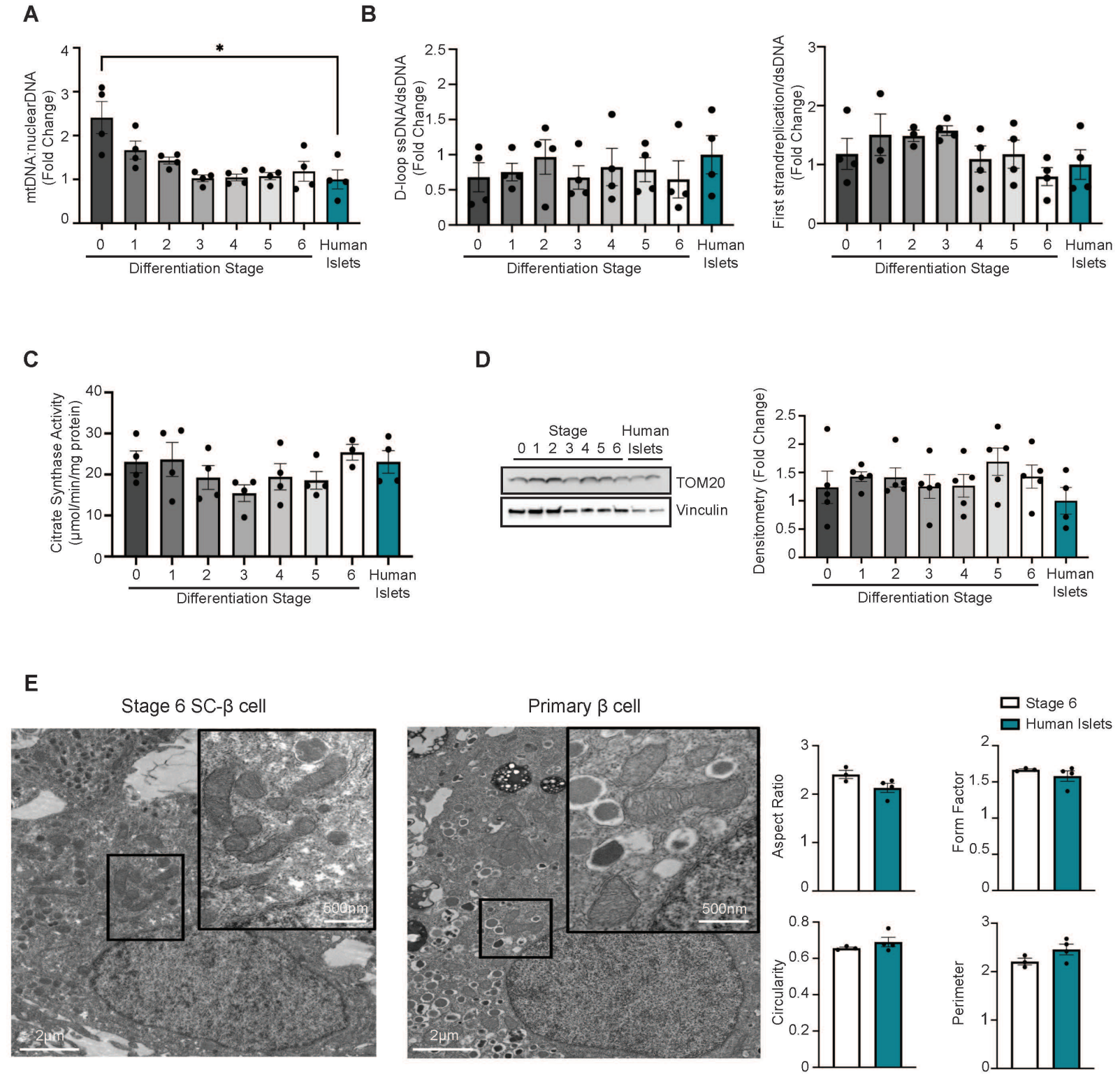
A
mtDNA:nuclearDNA (Fold Change)
*
0 1 2 3 4 5 6 Human Islets
Differentiation Stage
B
D-loop ssDNA/dsDNA (Fold Change)
First strandreplication/dsDNA (Fold Change)
C
Citrate Synthase Activity (µmol/min/mg protein)
D
Stage
Human Islets
TOM20
Vinculin
Densitometry (Fold Change)
E
Stage 6 SC-β cell
Primary β cell
500nm
2µm
Stage 6
Human Islets
Aspect Ratio
Form Factor
Circularity
Perimeter

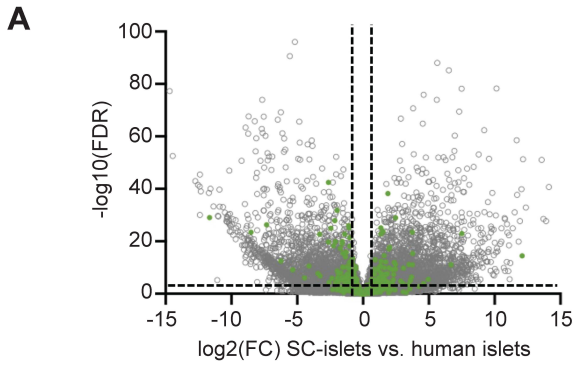

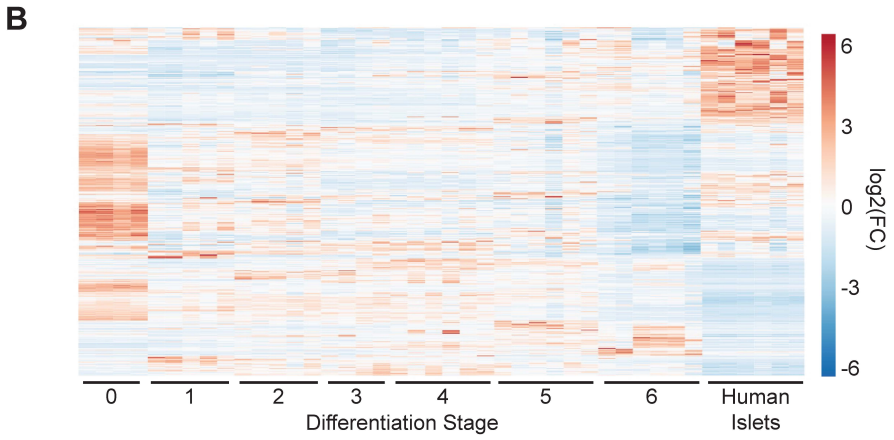

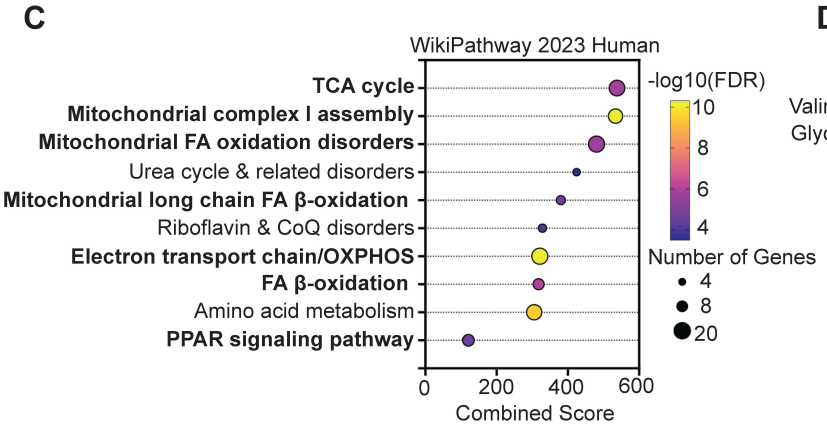

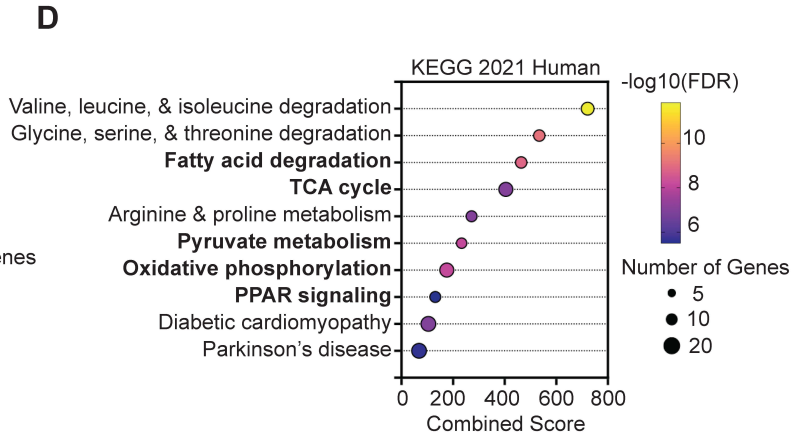

E

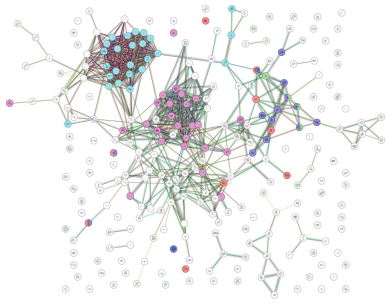

Biologic Process (Gene Ontology)	FDR
Mitochondrial Translation (GO:0032543)	1.83E-18
Oxidative Phosphorylation (GO:0006119)	9.11E-18
Cellular Lipid Catabolic Process (GO:0044242)	1.50E-05
Fatty Acid Biosynthetic Process (GO:0006633)	5.40E-03
Carnitine Metabolic Process (GO:0009437)	6.10E-03

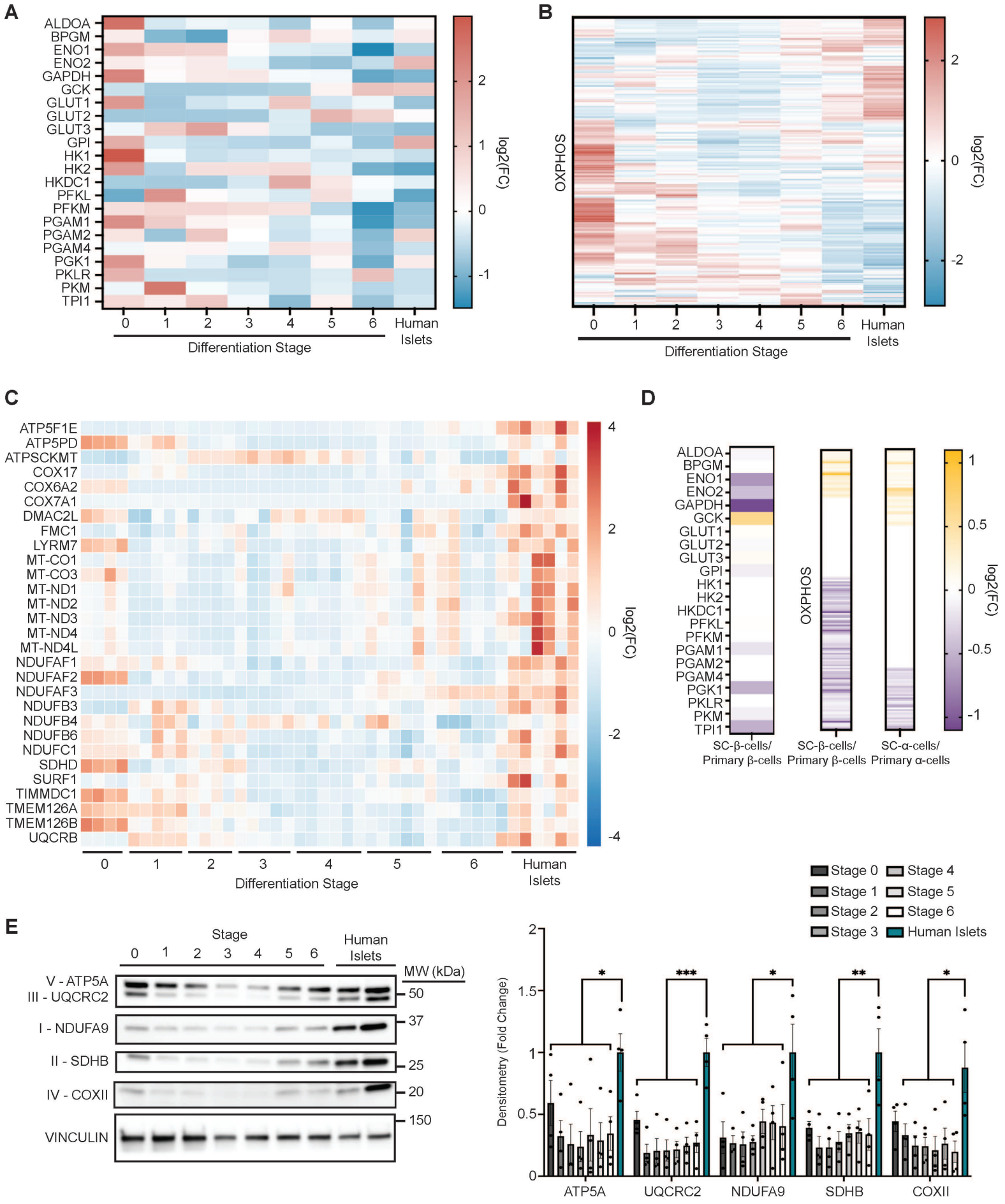
A
ALDOA
BPGM
ENO1
ENO2
GAPDH
GCK
GLUT1
GLUT2
GLUT3
GPI
HK1
HK2
HKDC1
PFKL
PFKM
PGAM1
PGAM2
PGAM4
PGK1
PKLR
PKM
TPI1
0 1 2 3 4 5 6 Human Islets
Differentiation Stage
log2(FC)
B
OXPHOS
0 1 2 3 4 5 6 Human Islets
Differentiation Stage
log2(FC)
C
ATP5F1E
ATP5PD
ATPSCKMT
COX17
COX6A2
COX7A1
DMAC2L
FMC1
LYRM7
MT-CO1
MT-CO3
MT-ND1
MT-ND2
MT-ND3
MT-ND4
MT-ND4L
NDUFAF1
NDUFAF2
NDUFAF3
NDUFB3
NDUFB4
NDUFB6
NDUFC1
SDHD
SURF1
TIMMDC1
TMEM126A
TMEM126B
UQCRB
0 1 2 3 4 5 6 Human Islets
Differentiation Stage
log2(FC)
D
ALDOA
BPGM
ENO1
ENO2
GAPDH
GCK
GLUT1
GLUT2
GLUT3
GPI
HK1
HK2
HKDC1
PFKL
PFKM
PGAM1
PGAM2
PGAM4
PGK1
PKLR
PKM
TPI1
OXPHOS
SC-β-cells/ Primary β-cells
SC-β-cells/ Primary β-cells
SC-α-cells/ Primary α-cells
log2(FC)
E
Stage
0 1 2 3 4 5 6 Human Islets
MW (kDa)
V - ATP5A
III - UQCRC2
I - NDUFA9
II - SDHB
IV - COXII
VINCULIN
50
37
25
20
150
Stage 0
Stage 1
Stage 2
Stage 3
Stage 4
Stage 5
Stage 6
Human Islets
Densitometry (Fold Change)
ATP5A
UQCRC2
NDUFA9
SDHB
COXII

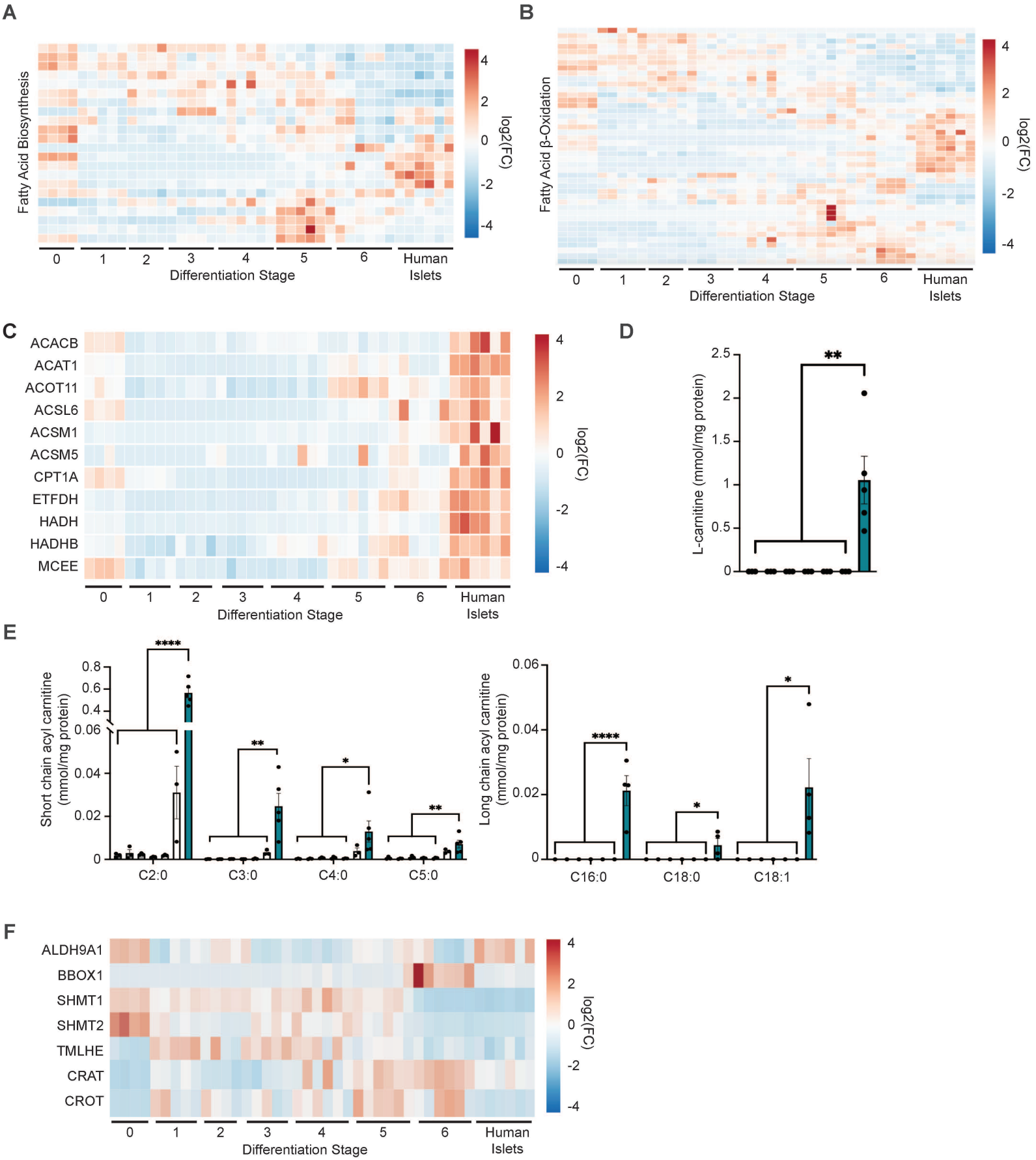
A
Fatty Acid Biosynthesis
log2(FC)
4
2
0
-2
-4
0
1
2
3
4
5
6
Human Islets
Differentiation Stage
B
Fatty Acid β-Oxidation
log2(FC)
Differentiation Stage
C
ACACB
ACAT1
ACOT11
ACSL6
ACSM1
ACSM5
CPT1A
ETFDH
HADH
HADHB
MCEE
log2(FC)
Differentiation Stage
D
L-carnitine (mmol/mg protein)
2.5
2
1.5
1
0.5
0
**
E
Short chain acyl carnitine (mmol/mg protein)
0.8
0.6
0.4
0.06
0.04
0.02
0
****
**
*
**
C2:0
C3:0
C4:0
C5:0
Long chain acyl carnitine (mmol/mg protein)
0.06
0.04
0.02
0
****
*
*
C16:0
C18:0
C18:1
F
ALDH9A1
BBOX1
SHMT1
SHMT2
TMLHE
CRAT
CROT
log2(FC)
Differentiation Stage

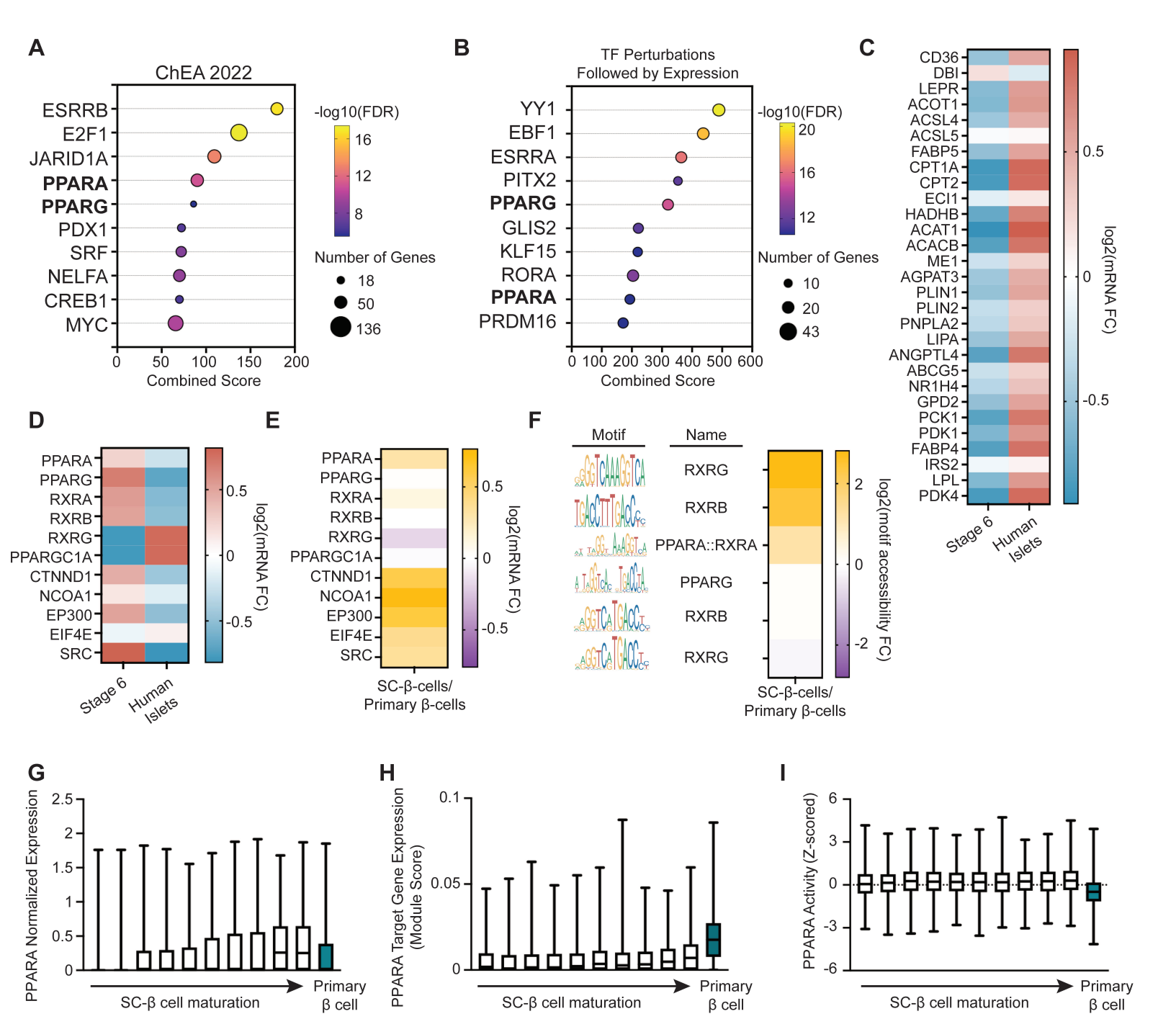
A
ChEA 2022
ESRRB
E2F1
JARID1A
PPARA
PPARG
PDX1
SRF
NELFA
CREB1
MYC
0 50 100 150 200
Combined Score
-log10(FDR)
16
12
8
Number of Genes
18
50
136
B
TF Perturbations
Followed by Expression
YY1
EBF1
ESRRA
PITX2
PPARG
GLIS2
KLF15
RORA
PPARA
PRDM16
0 100 200 300 400 500 600
Combined Score
-log10(FDR)
20
16
12
Number of Genes
10
20
43
C
CD36
DBI
LEPR
ACOT1
ACSL4
ACSL5
FABP5
CPT1A
CPT2
ECI1
HADHB
ACAT1
ACACB
ME1
AGPAT3
PLIN1
PLIN2
PNPLA2
LIPA
ANGPTL4
ABCG5
NR1H4
GPD2
PCK1
PDK1
FABP4
IRS2
LPL
PDK4
0.5
0
-0.5
log2(mRNA FC)
Stage 6
Human Islets
D
PPARA
PPARG
RXRA
RXRB
RXRG
PPARGC1A
CTNND1
NCOA1
EP300
EIF4E
SRC
0.5
0
-0.5
log2(mRNA FC)
Stage 6
Human Islets
E
PPARA
PPARG
RXRA
RXRB
RXRG
PPARGC1A
CTNND1
NCOA1
EP300
EIF4E
SRC
0.5
0
-0.5
log2(mRNA FC)
SC-β-cells/
Primary β-cells
F
Motif
Name
RXRG
RXRB
PPARA::RXRA
PPARG
RXRB
RXRG
2
0
-2
log2(motif accessibility FC)
SC-β-cells/
Primary β-cells
G
PPARA Normalized Expression
2.5
2
1.5
1
0.5
0
SC-β cell maturation
Primary
β cell
H
PPARA Target Gene Expression
(Module Score)
0.1
0.05
0
SC-β cell maturation
Primary
β cell
I
PPARA Activity (Z-scored)
6
3
0
-3
-6
SC-β cell maturation
Primary
β cell

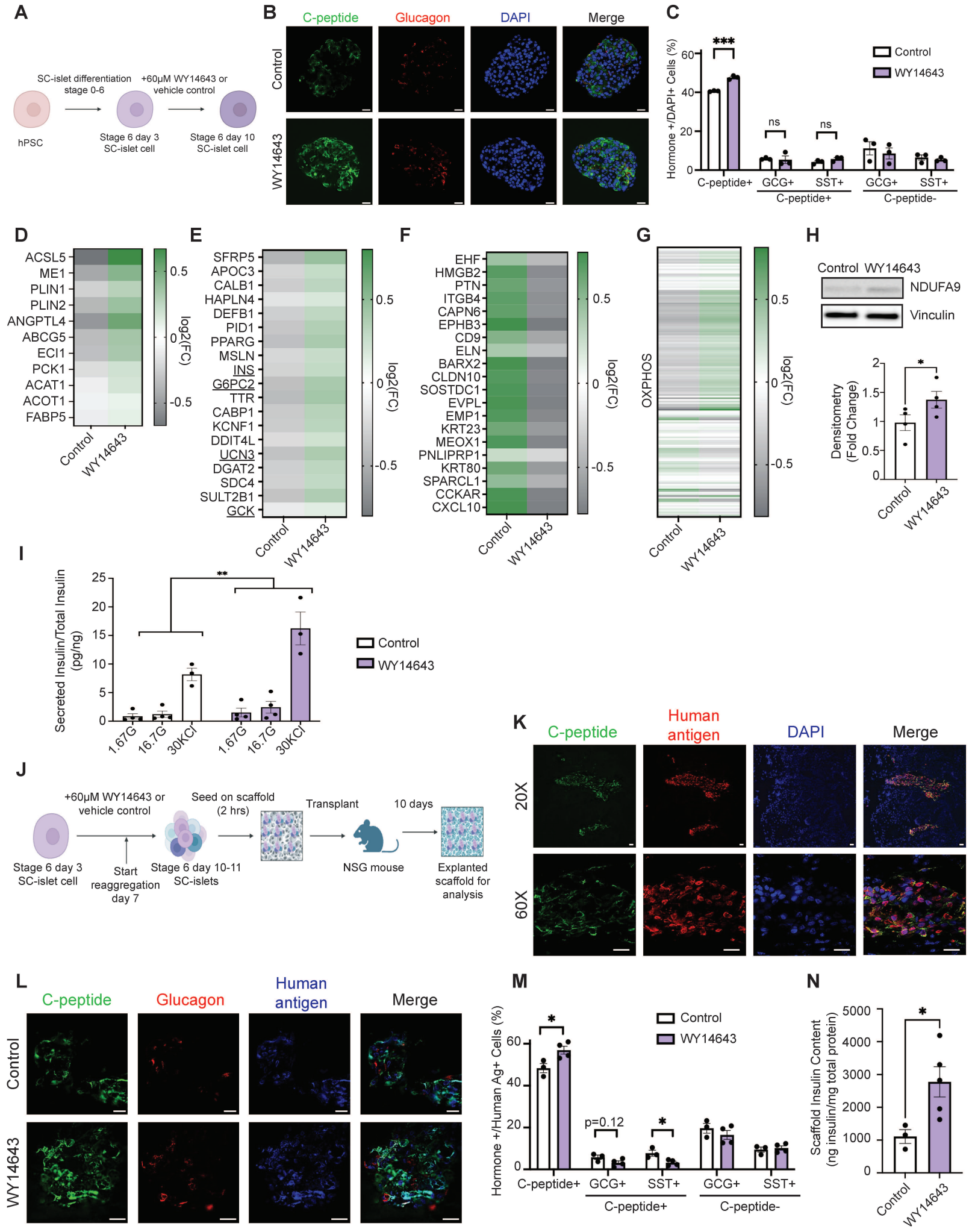
A
SC-islet differentiation stage 0-6
+60μM WY14643 or vehicle control
hPSC
Stage 6 day 3 SC-islet cell
Stage 6 day 10 SC-islet cell
B
C-peptide
Glucagon
DAPI
Merge
Control
WY14643
C
Hormone +/DAPI+ Cells (%)
***
ns
ns
Control
WY14643
C-peptide+
GCG+
SST+
GCG+
SST+
C-peptide+
C-peptide-
D
ACSL5
ME1
PLIN1
PLIN2
ANGPTL4
ABCG5
ECI1
PCK1
ACAT1
ACOT1
FABP5
log2(FC)
Control
WY14643
E
SFRP5
APOC3
CALB1
HAPLN4
DEFB1
PID1
PPARG
MSLN
INS
G6PC2
TTR
CABP1
KCNF1
DDIT4L
UCN3
DGAT2
SDC4
SULT2B1
GCK
log2(FC)
Control
WY14643
F
EHF
HMGB2
PTN
ITGB4
CAPN6
EPHB3
CD9
ELN
BARX2
CLDN10
SOSTDC1
EVPL
EMP1
KRT23
MEOX1
PNLIPRP1
KRT80
SPARCL1
CCKAR
CXCL10
log2(FC)
Control
WY14643
G
OXPHOS
log2(FC)
Control
WY14643
H
Control
WY14643
NDUFA9
Vinculin
Densitometry (Fold Change)
*
Control
WY14643
I
Secreted Insulin/Total Insulin (pg/ng)
**
1.67G
16.7G
30KCl
1.67G
16.7G
30KCl
Control
WY14643
J
+60μM WY14643 or vehicle control
Seed on scaffold (2 hrs)
Transplant
10 days
Stage 6 day 3 SC-islet cell
Start reaggregation day 7
Stage 6 day 10-11 SC-islets
NSG mouse
Explanted scaffold for analysis
K
C-peptide
Human antigen
DAPI
Merge
20X
60X
L
C-peptide
Glucagon
Human antigen
Merge
Control
WY14643
M
Hormone +/Human Ag+ Cells (%)
*
p=0.12
*
Control
WY14643
C-peptide+
GCG+
SST+
GCG+
SST+
C-peptide+
C-peptide-
N
Scaffold Insulin Content (ng insulin/mg total protein)
*
Control
WY14643